PLOS Computational Biology

RESEARCH ARTICLE

In silico clinical trials of BiTE expression by oncolytic viruses reveal the impact of patient heterogeneity on dosage protocol

Adrianne L. Jenner[1]*, Robyn P. Araujo[2], Noa L. Levi[2], Guy Ungerechts[3,4,5], Christine E. Engeland[6], Johannes P. W. Heidbuechel[3,4]

1 School of Mathematical Sciences, Queensland University of Technology, Brisbane, Queensland, Australia, **2** School of Mathematics and Statistics, University of Melbourne, Melbourne, Victoria, Australia, **3** Clinical Cooperation Unit "Virotherapy", German Cancer Research Center (DKFZ), Heidelberg, Germany, **4** National Center for Tumor Diseases (NCT), NCT Heidelberg, a partnership between DKFZ and Heidelberg University Hospital, Heidelberg, Germany, **5** Department of Medical Oncology, Heidelberg University Hospital, Medical Faculty Heidelberg, Heidelberg University, Heidelberg, Germany, **6** Experimental Hematology and Immunotherapy, Department of Hematology, Hemostaseology, Cellular Therapy and Infectious Diseases, Faculty of Medicine and Leipzig University Hospital, Fraunhofer Institute for Cell Therapy and Immunology (IZI), Leipzig, Germany

* adrianne.jenner@qut.edu.au

Check for updates

OPEN ACCESS

Citation: Jenner AL, Araujo RP, Levi NL, Ungerechts G, Engeland CE, Heidbuechel JPW (2026) In silico clinical trials of BiTE expression by oncolytic viruses reveal the impact of patient heterogeneity on dosage protocol. PLoS Comput Biol 22(7): e1014533. https://doi.org/10.1371/journal.pcbi.1014533

Editor: David Basanta Gutierrez, Moffitt Cancer Center, UNITED STATES OF AMERICA

Received: February 2, 2026

Accepted: July 5, 2026

Published: July 30, 2026

Peer Review History: PLOS recognizes the benefits of transparency in the peer review process; therefore, we enable the publication of all of the content of peer review and author responses alongside final, published articles. The editorial history of this article is available here: https://doi.org/10.1371/journal.pcbi.1014533

Copyright: © 2026 Jenner et al. This is an open access article distributed under the terms of the Creative Commons Attribution License, which permits unrestricted use, distribution,

Abstract

Immunotherapies have become a transformative therapeutic strategy for many cancer types in recent years. Bispecific T-cell engagers (BiTEs) are one promising immunotherapy that enhances cellular antitumour immunity by redirecting T cells towards cancer cells. Recent evidence suggests that BiTE efficacy can be augmented by encoding BiTEs in oncolytic measles virus vectors (MV-BiTE). Infection of cancer cells with MV-BiTE causes the local production of BiTEs and has shown safety and efficacy in murine tumour models. However, whether the observed efficacy of this treatment will translate to a heterogeneous human population is unknown. In this work, we generate an *in silico* clinical trial of MV-BiTE therapy using a system of ordinary differential equations. We capture potential heterogeneity of individual patients using variability in *in vivo* tumour volume and change in baseline (%) measurements from a Phase II clinical trial. In lieu of human MV-BiTE data, we use the oncolytic virus talimogene laherparepvec (T-VEC) as a surrogate oncolytic virus carrying an immunostimulatory payload. Our predictions imply that the main drivers of heterogeneity are the underlying effector T cell killing rate and BiTE pharmacokinetics. Furthermore, we find that if individuals are classified as non-responders to the Phase II T-VEC clinical protocol, they may respond to more frequent administration of lower dosages. This work highlights how *in silico* clinical trials can provide predictions for novel therapeutics to generate hypotheses and guide the design of treatment schedules for clinical translation.

and reproduction in any medium, provided the original author and source are credited.

Data availability statement: The code generated for this study can be found in the https://github.com/AdrianneJennerQUT/insilico-clinical-trial-MV-BiTEs.

Funding: ALJ acknowledges funding and support from the Discovery Early Career Award DE240100650 and the QUT Women in STEM Writing Retreat. RPA acknowledges funding and support from an Australian Research Council (ARC) Discovery Project (project no. DP230100485) from the Australian Government. NLL acknowledges support from the QUT Centre for Data Science First Byte Scheme and the ANZIAM AF Pillow Award. CEE acknowledges funding support from the German National Science Foundation (DFG), Grant EN-1119/2-2, Wilhelm Sander Foundation Grant 2018.058.01. JPWH was supported by a research grant from the "Stiftung für Krebs- und Scharlachforschung" awarded by the Medical Faculty Heidelberg, Heidelberg University, and by a postdoctoral fellowship from the Heidelberg School of Oncology (HSO) at the National Center for Tumor Diseases (NCT) Heidelberg. The funders had no role in study design, data collection and analysis, decision to publish, or preparation of the manuscript.

Competing interests: I have read the journal's policy and the authors of this manuscript have the following competing interests: Dr Engeland is listed as inventor on patents filed by her former institution describing immunomodulatory oncolytic viruses. G.U. is founder and current CMO/CSO of CanVirex, Basel, Switzerland and reports grants or contracts from DFG, German Cancer Aid, and Wilhelm Sander Foundation and consulting fees from Boehringer Ingelheim. Apart from this, the authors declare that the research was conducted in the absence of any commercial or financial relationships that could be construed as a potential conflict of interest.

Author summary

The immune system has the ability to kill cancer cells; however, cancer cells are able to resist immune cell-mediated killing. A new therapy uses modified measles viruses to activate the immune system against cancer. These viruses are modified with bispecific T-cell engagers (BiTEs) which assist immune cells in targeting and removing cancer cells. While the potential success of this treatment has been demonstrated in mouse models, it is yet to be verified in a human cohort. In this work, we use mathematical and computational simulations to examine how patient-to-patient variability might affect the success of this treatment. We compare our model predictions to data from a clinical trial and find that virtual individuals in the simulation that are classified as non-responders to the standard protocol would likely respond better to more frequent administrations of lower dosages. The work presented here generates hypotheses for how individuals in a human cohort may respond, however, more work is required to verify these results in humans.

Introduction

Over the past few decades, the treatment of cancer has significantly improved with the introduction of immunotherapies [1]. Broadly speaking, immunotherapies work by eliciting the activity of the patient's own immune system to recognise and destroy cancer cells. Within the field of immunotherapies, one treatment avenue has been T cell retargeting [2,3] which aims to bring cytotoxic T lymphocytes into contact with target tumour cells so that cytotoxic responses can be triggered. Bispecific T cell engager® (BiTE) molecules are a recently introduced class of immunotherapeutics that mediate T cell retargeting [2,4,5]. Similar to chimeric antigen receptor (CAR) T cell therapy [6], these molecules induce T cell binding to tumour cells by forming cytolytic synapses between T cells and tumour cells, irrespective of T cell receptor specificity and independent of co-stimulation. Unlike standard antibodies, BiTEs have dual antigen specificity, allowing them to bind to two unique antigens and thereby facilitate targeted cell-to-cell interactions [2,3]. BiTEs are designed to target the T cell antigen CD3 and a tumour-specific antigen simultaneously and promote the cytotoxicity of T cells via crosslinking with tumour cells [4].

Bispecific T cell-recruiting antibodies have been approved for the treatment of haematological malignancies, such as CD19-targeting blinatumomab, approved first-in-class in 2014, while many more are in clinical trials [7–11]. Unfortunately, limited bioavailability and severe toxicities have hampered broader clinical application, especially against solid tumours [12]. Fortunately, oncolytic viruses (OVs) can serve as vectors to deliver BiTEs to solid tumours [12–19], reducing systemic toxicity issues (Fig 1). OVs are naturally occurring or genetically modified viruses which preferentially infect and replicate in tumour cells. Following viral replication, the cell lyses (bursts), releasing the newly generated virions. OVs stimulate an antiviral immune

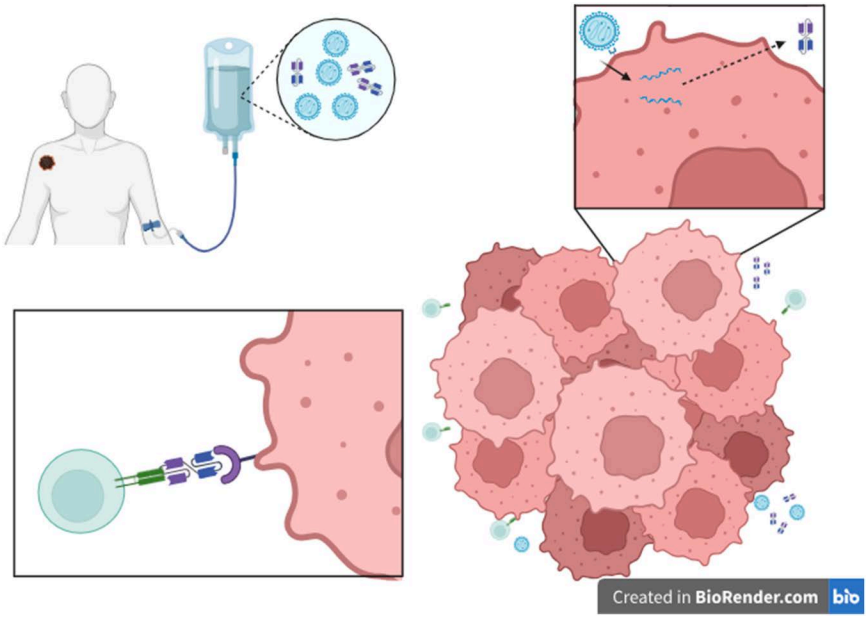

Fig 1. Oncolytic measles viruses encoding bispecific T cell engagers (MV-BiTEs) in the treatment of cancer. MV-BiTEs are administered intratumourally. In pre-clinical studies, due to the virus production method, the suspension may also contain free BiTEs. MV-BiTE-infected tumour cells express and secrete BiTE antibodies. Infected cells ultimately die through tumour cell lysis. T cells are recruited by immune cells sensing the viral infection and by the presence of BiTEs. Simultaneous association of BiTEs with T cells and tumour antigens mediates T cell cytotoxicity against non-infected tumour cells as a bystander effect. Created in BioRender. Engeland, C. (2026). https://BioRender.com/5y7xc38.

https://doi.org/10.1371/journal.pcbi.1014533.g001

response as well as an antitumour immune response [20]. Potential synergistic effects of BiTE-encoding OVs (OV-BiTEs) result from the inherent ability of the immune system to respond to viral infections, and in doing so, promote the recruitment of T cells to the tumour site which allows for BiTE engagement. Efficacy of the OV-BiTE approach against solid tumours has been postulated by several groups [21–24]. In particular, a recent review [12] highlighted that further demonstration of the applicability and efficacy of OV-BiTEs in a clinical setting is needed as well as investigation of combination therapies [15,24].

Mathematical modelling of novel cancer treatments has been a prominent resource in biomedical and cancer research for some time [25,26]. In particular, a specific focus has been on using mathematics to improve oncolytic virotherapies and immunotherapies [19,24,27–32]. Deterministic systems of ordinary differential equations (ODEs) have been employed to investigate novel OV derivatives and the ways in which the resulting antiviral immune response can be harnessed [28,33–36]. The *in vitro* dose-response relationship of CD3-bispecific antibodies has been examined using a mathematical model [37]. More recently, the first ordinary differential equation system capturing OV-BiTEs was created [27]. While deterministic models are advantageous in their ability to capture mean-field dynamics of a given biological phenomenon, they do not explicitly incorporate heterogeneity that may exist across a cancer patient cohort. To account for this variation in patient characteristics, a virtual clinical trial (VCT) or *in silico* clinical trial can be used [38–40]. There are many examples of VCTs applied to cancer therapies [33,41–44] and novel techniques are being developed that assist in virtual patient generation and parameter estimation [40,45,46].

In this work, we develop an ODE system to represent the action of OV-BiTEs injected intratumourally that subsequently kill tumour cells and stimulate an antitumour immune response. We fit parameters in the model to *in vitro*

and *in vivo* measurements for oncolytic measles virus (MV) encoding BiTEs (MV-BiTE) [13]. As there is no human clinical trial data available for MV-BiTE, we generated populations of virtual patients and investigated the efficacy of this therapy in a virtual clinical trial. We focus our attention on understanding whether an optimal dosage protocol exists for a cohort of heterogeneous individuals, or whether there are individual characteristics that will lead to a more effective treatment. We show that with a simple, cost-effective mathematical simulation we can capture human variations in response to treatment and predict the effectiveness of protocols, which could serve as a useful pre-clinical trial step.

Materials and methods

Mathematical model

To better understand MV-BiTE therapy, we generated a system of ordinary differential equations (ODEs) based on previous models for the immune response to immunostimulatory oncolytic viruses [47,48]. Our model captures a growing uninfected population of tumour cells, $U(t)$, that become infected by MV-BiTEs, $V(t)$ and lyse. Inside infected tumour cells, the virus replicates, leading to the production of BiTEs, $B(t)$, which are released upon cell lysis. The presence of dead cells or cell debris $D(t)$ stimulates the recruitment of effector CD3$^+$ T cells $T(t)$ to the tumour site. T cells can then induce apoptosis in tumour cells. The presence of BiTEs increases the ability of effector T cells to induce apoptosis in tumour cells. These dynamics are captured in Fig 2, Tables 1 and 2 and the system of ODEs below:

$$\frac{\mathrm{d}U}{\mathrm{d}t} = rU\log\left(\frac{L}{U}\right) - \frac{\beta UV}{U+\eta} - \frac{kUT}{N}\left(\epsilon + \frac{B}{B+\gamma}\right), \tag{1}$$

$$\frac{\mathrm{d}D}{\mathrm{d}t} = \frac{\beta UV}{U+\eta} + \frac{kUT}{N}\left(\epsilon + \frac{B}{B+\gamma}\right) - d_D D, \tag{2}$$

$$\frac{\mathrm{d}V}{\mathrm{d}t} = \frac{\beta UV}{U+\eta} - d_V V, \tag{3}$$

$$\frac{\mathrm{d}B}{\mathrm{d}t} = \alpha_B \frac{\beta UV}{U+\eta} - d_B B, \tag{4}$$

$$\frac{\mathrm{d}T}{\mathrm{d}t} = sD - d_T T, \tag{5}$$

where t is time and $N = U + D + T$. To keep the units consistent throughout the model, V is in units *cells* which is converted to a quantity of virions by $V^* = \alpha_V V$, where α_V has units *virions*/*cell* and V^* has units virions. For further examples of mathematical models that capture the immune response to oncolytic virotherapy and the resulting antitumour effect, see [28,34].

In Eq. 1, tumour cells, $U(t)$, grow under a Gompertzian tumour growth law [49], under which cells proliferate at rate r and the population will grow until a certain carrying capacity L is reached. The carrying capacity is a representative of the tumour growth trajectory and does not represent the termination criteria, which may be reached at a smaller value. Tumour cells become infected and undergo lysis at a rate β. These infected cells can form syncytia, which we have chosen not to explicitly model here. Infection is modelled as proportional to the concentration of virus and a Michaelis-Menten function with the concentration η giving 50% of the maximum infectivity, also known as the half-effect. We introduce this infection term to capture that virus penetration into a tumour is often inhibited spatially either due to the microenvironment or otherwise [50]; see [35,41,51] for similar uses of this infectivity formulation. Tumour cells undergo T cell-induced apoptosis at a frequency-dependent rate with constant

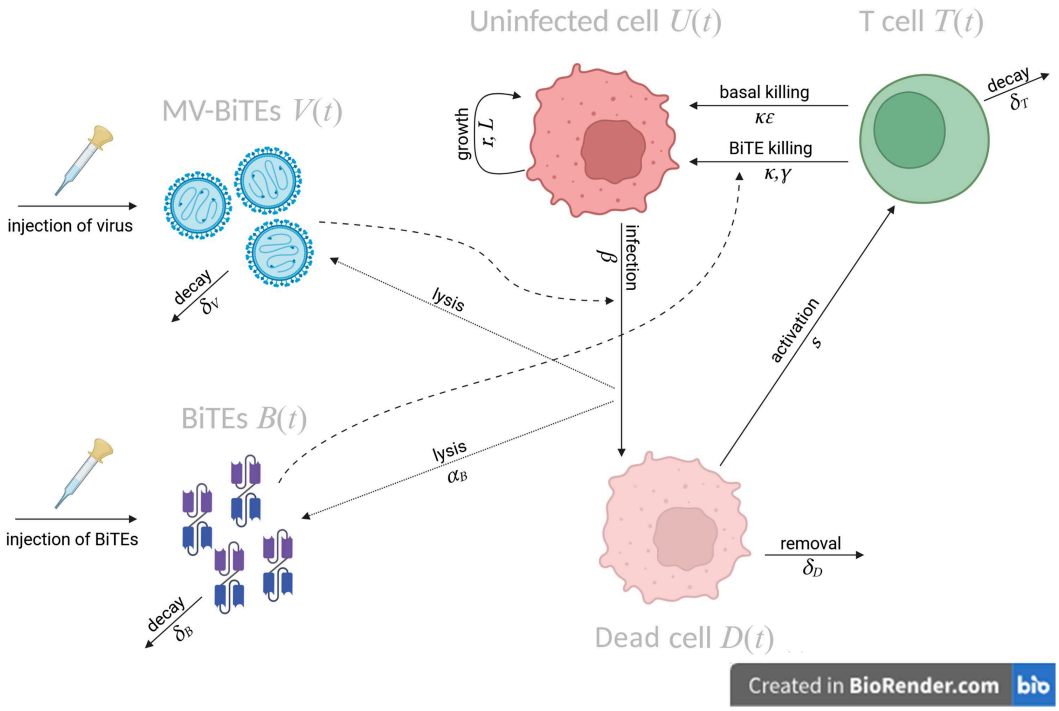

Fig 2. Schematic for the mathematical model in Eqs. 1–5 describing MV-BiTEs. Viruses $V(t)$, genetically engineered to encode BiTEs, are injected into the system and infect uninfected tumour cells $U(t)$. These cells eventually die, becoming dead cells, $D(t)$ and release new viruses and BiTEs $B(t)$ to the tumour environment. The presence of dead cells activates and recruits CD3⁺ T cells $T(t)$. T cells induce apoptosis in cancer cells. The presence of BiTEs increases the ability of T cells to induce apoptosis in uninfected tumour cells. Created in BioRender. Engeland, C. (2026). https://BioRender.com/ia6sdw3.

https://doi.org/10.1371/journal.pcbi.1014533.g002

Table 1. Summary of variables in Eqs. 1–5.

Variable	Units	Description
U	cells	Not-productively infected (uninfected, eclipse – not secreting BiTEs/virus) pool of cells.
D	cells	Productively infected pool of cells producing BiTEs/virus that ultimately die.
V^*	virions	Number of oncolytic measles virions, note $V^* = \alpha_V V$.
B	μg/ml	BiTE (Bispecific T cell engager) concentration.
T	cells	CD3⁺ T cells.

https://doi.org/10.1371/journal.pcbi.1014533.t001

k. For uses of frequency-dependent terms in OV modelling similar to this, see [47,48,52]. To model the effect of BiTEs on T cell activity, we assume a baseline T cell apoptosis factor ϵ, and that BiTE-mediated killing is an additional factor on top of this baseline killing rate, modelled using a Michaelis-Menten term with half-effect γ.

We have removed the intermediate 'infected' population that is often present in models of viral infections [28,34,47,53,54] and instead have direct generation of virus and BiTEs through infection of tumour cells, similar to [55], so that production of BiTEs is modelled continuously over time and not in discrete bursts. We found that introducing the infected cell pool and its specific lysis rate introduced both structural and practical identifiability issues into the model. We also assume infected cells do not replicate after infection, meaning the process of infection is terminal for a cell. In this way, we capture the process of infection, lysis and immune cell recruitment through one population $D(t)$.

Table 2. Parameters for Eqs. 1–5.Estimates were obtained through fitting to in vitro and in vivo data with parameters having different values in vitro (top row) and in vivo (bottom row). Other measurements were estimated based on literature, with their reference given. For the annotation of the experiments below they correspond to the following experiments detailed in the methods: "progeny" - Viral replication kinetics (S1 Fig), "viability" - Virus-mediated (onco-)lysis:cell viability (S1 Fig), "lysis" – BiTE-mediated (T cell) cytotoxicity: specific lysis (S2 Fig), "tumour volume" – in vivo tumour volume (Fig 4).

Parameter	Units	Description	Value	Reference	Experiment
r	1/day	proliferation rate of cancer cells	0.004	S1 Fig	viability, progeny.
			0.1321	Fig 4B	tumour volume
L	cells	carrying capacity of tumour	2.73×10^9	Fig 4B	tumour volume
β	1/day	infectivity rate	270.8	S1 Fig	viability, progeny.
			25	S1 Fig	viability, progeny.
η	cells	infection half-effect	9.04×10^5	S1 Fig	viability, progeny.
k	1/day	T cell killing rate	0.1973	S2 Fig	lysis.
			0.2567	Fig 4C–4E	tumour volume
ϵ	–	basal T cell killing constant	0.1716	S2 Fig	lysis.
			0.98	Fig 4C–4E	tumour volume
γ	μg/ml	BiTE half-effect	4.25×10^{-3}	S2 Fig	lysis.
d_D	1/day	dead cell disintegration	5.8	Fig 4C–4E	tumour volume
d_V	1/day	virus decay	23.11	S1 Fig	viability, progeny.
α_V	virions/cell	viruses per cell	100.56	S1 Fig	viability, progeny.
α_B	BiTEs/cell	BiTE production	4.6×10^4	Fig 4C–4E	tumour volume
d_B	1/day	decay rate of BiTEs	2.65	Fig 4C–4E	tumour volume
s	1/day	stimulation of T cells	28.7	Fig 4C–4E	tumour volume
d_T	1/day	decay rate of T cells	0.35	[47]	

https://doi.org/10.1371/journal.pcbi.1014533.t002

In Eq. 2, we track the accumulation of dead cells or dead cell debris, $D(t)$, through the induction of lysis by an OV or apoptosis by T cells. To promote the practical identifiability of our model, we chose not to explicitly capture the production of tumour or viral antigens, subsequent activation of antigen-presenting cells, cytokine/chemokine production and then T cell recruitment. As such, we use the accumulation of dead cells and debris as a proxy for this process. Dead cell debris is produced at the same rate that tumour cells die and is removed (decays) from the system at a rate d_D.

In Eq. 3, new viruses are produced through virus infection of tumour cells. These are assumed to decay due to factors such as adaptive immune cell clearance, complement clearance, and sequestration, for example, by the reticuloendothelial system at a rate d_V. As each cell produces α_V virions, we scale the rate of production and decay of virions by α_V to obtain an estimate for the number of virions, $V^*(t)$.

In Eq. 4, through cell lysis, α_B new BiTEs, $B(t)$, are released. These BiTEs decay at a rate d_B, i.e., a pharmacokinetic parame*t*er. We assume that these BiTEs consist of both T cell-bound and free BiTEs in the local tumour microenvironment (TME). While BiTEs can be secreted throughout the lifetime of the cell, we found separating the number of BiTEs released at lysis α_B from the amount secreted up to lysis was not structurally identifiable with the given experimental measurements. As such, we assume that any BiTEs released up to lysis are included in the amount secreted at lysis α_B.

In Eq. 5, T cells, $T(t)$, accumulate at the tumour site based on the presence of dead cell debris at a rate s. These cells also decay at a rate d_T. We assume T cells are recruited at a rate sD, which can be thought of as a proxy for antigen-presenting cell activation by viral antigens or tumour antigens, downstream stimulation of T cells in the lymph nodes, and tumour-directed T cell chemotaxis.

The model was simulated in MATLAB and solved numerically using *ode45*. Initial conditions are given below:

$$U(0) = U_0, \quad D(0) = 0, \quad V(0) = V_I, \quad B(0) = B_I, \quad T(0) = T_0.$$

The model was solved piecewise to simulate n injections of BiTEs B_0 and virus V_0 at time t_I:

$$V(t_I) = V(t_I) + V_I, \quad B(t_I) = B(t_I) + B_I,$$

for $I = 1,...,n$.

Structural and practical identifiability

Identifiability is an important component of mathematical modelling as it determines the capacity of a model to extract parameter estimates from data [56–59]. This is particularly important in biology, where parameterised models are used to make predictions about living systems [60,61]. We refined the model presented in Eqs. 1–5 numerous times to minimise identifiability issues. The model was found to be structurally identifiable using the open-source software DAISY [62,63]. Structural identifiability implies practical identifiability only for infinite data [56]. For finite data samples, there are numerous ways to evaluate practical identifiability [64–66]; for our dataset and model, we have analysed practical identifiability with a global and local sensitivity analysis.

Details of experimental and clinical measurements

To estimate parameters in Eqs. 1–5, we use a range of *in vitro* and *in vivo* experiments from oncolytic measles virus (MV) encoding and not encoding BiTEs [13], as well as a Phase II clinical trial for talimogene laherparepvec (T-VEC) [67]. Vaccine-derived, live attenuated MV vectors were designed based on established reverse genetics systems and were generated to encode BiTEs targeting murine CD3 and human CD20 [68]. For *in vitro* studies and the syngeneic subcutaneous tumour model in C57Bl/6J mice, murine melanoma-derived B16-CD20-CD46 cells stably expressing the BiTE target antigen human CD20 and human CD46 as entry receptor for oncolytic measles virus were used.

Viral replication kinetics. Replication kinetics of MV were captured by determining the viral progeny produced in B16-CD20-CD46. 10^5 cells on 12-well plates were inoculated with the same dose (multiplicity of infection, MOI of 1) of cell infectious units (ciu) of MV encoding mCD3xCD20-BiTE (with one scFv targeting murine CD3 expressed on mouse T cells and the other recognizing the human CD20 antigen) for 12 hours. Inoculum was then replaced by medium. At designated time points, supernatants were collected, samples were frozen and viral progeny was assessed via serial dilution titration assay.

Virus-mediated (onco-)lysis: Cell viability. Cytotoxic effects of MV were determined in B16-CD20-CD46 cells. The cells were infected with unmodified MV at an MOI of 1 as for the replication assay and cell viability was determined by metabolic XTT assay every 12 hours for 96 hours. Viability was calculated relative to mock-infected cells.

BiTE-mediated (T cell) cytotoxicity: Specific lysis. T cell cytotoxicity mediated by BiTEs was determined in B16-CD20-CD46 tumour cells expressing the BiTE target antigen co-cultured with primary, unstimulated immune effector cells obtained from mouse spleens at varying BiTE concentrations. Three experiments with independently produced mCD3xCD20 BiTE batches purified from the supernatant of MV-mCD3xCD20-infected (Vero producer) cells were performed. LDH release was determined at 44h after setting up the co-cultures and specific tumour cell lysis was calculated relative to chemically lysed maximum release controls following subtraction of background values taken from target cell only and effector cell only controls, as described in Heidbuechel and Engeland [12] and Speck *et al.* [13].

***In vivo* tumour volume.** For *in vivo* experiments, C57/BL6J mice were injected with 10^6 B16-CD20-CD46 cells s.c. After tumour engraftment, mice were stratified to respective treatment groups according to tumour size and treated with intratumoural injections. The experimenter was blinded to treatment groups. Treatment conditions included carrier fluid only (mock), purified BiTE (mCD3xCD20, as in the LDH release assay), unmodified measles virus (MV), and MV encoding CD20-targeting BiTE (MV-mCD3xCD20). The injection protocol was 5 intratumoural injections administered on consecutive days of 100μL volume each containing 10^6 cell infectious units (i.e., infectious virus as assessed by titration). In the respective "BiTE only" treatment group, 2.17μg of purified BiTE (in 100μL suspension) was injected 5x instead

of virus, which corresponds to what was found to be present in 100μL of MV-BiTE suspension via flow cytometry in a quantitative binding assay. Note that the estimate of 2.17μg would depend on the injection and tumour volume, however, for simplicity we have assumed this as a fixed amount throughout our simulations.

Caliper measurements were performed every three days to determine tumour volume. Tumour volumes were calculated as [larger diameter $\times$ smaller diameter $\times$ smaller diameter]/2. All experiments were conducted with non-immunocompromised wild-type C57BL/6 mice with endogenous $CD3^+$ T cells. Intratumoural T cell abundance is known to be quite low in the B16 model [69] and increased upon treatment (more so in the MV-BiTE vs MV experiment as assessed by flow cytometry). If ulceration presented in the mice as the tumours formed, these mice were not included in this study.

Phase II Clinical Trial measurements for change from baseline (%). To evaluate the function of the model in a clinical setting, data from a Phase II T-VEC trial [67] was used. T-VEC is a herpes simplex virus type 1-derived oncolytic immunotherapy designed to selectively replicate within tumours and encode granulocyte-macrophage colony-stimulating factor (GM-CSF) to enhance systemic antitumour immune responses. Eligible patients were age $\geq$ 18 years with unresectable stage IIIB-IV melanoma. T-VEC was administered by intralesional injection following the dosing regimen described in the registrational Phase III OPTiM study [70], which was a first dose of T-VEC of 10^6 pfu/ml, followed by T-VEC doses of 10^8 pfu/ml 3 weeks after the first dose and then once every 2 weeks. Treatment continued for $\geq$ 6 months from initial dosing provided treatment was tolerated.

Parameter estimation

To estimate parameters in the model, a series of hierarchical parameter fits were conducted to *in vitro* and *in vivo* measurements using MATLAB's inbuilt non-linear least squares optimisation algorithm *lsqnonlin* and the inbuilt multistart algorithm *multistart*. The viral infection and replication parameters β, η, d_V and α were estimated using the *in vitro* viral progeny and cell viability experiments, see in S1 Text and S1 Fig. The BiTE and T cell killing parameters ϵ, k, and γ were obtained through fitting the specific lysis (%) data, S2 Fig. The *in vivo* tumour growth rate without treatment, r and L, were obtained through fitting to the control data set, assuming that 10^6 cells were injected at day 0 and $1mm^3 = 10^6$ cells [71].

Given the initial parameter estimates from the *in vitro* experiments, we then recalibrated parameters to the *in vivo* measurements. We simultaneously fit the model to the purified BiTEs, MV and MV-BiTEs measurements to obtain $\beta, k, \epsilon, d_D, \alpha_B, d_B$, and s. The decay rate of T cells was taken from data fitting, d_T = 0.35/day, [48]. The time from initiation of cell apoptosis to completion can occur as quickly as 2–3 hours. If we assume that debris can remain for another 2 hours after this, this gives a dead cell clearance rate of d_D= 4.8/day [72]. For fitting the *in vivo* data: $B(0)$ = 2.17μg, and $V(0)=10^6$ cells. Further details of each fit are provided in the Supplementary Material.

Sensitivity analysis

We evaluated the sensitivity of our model predictions to perturbations to the obtained parameter estimates through a local and global sensitivity analysis. We conducted a pairwise local sensitivity analysis around the fitted parameter values, see Supplementary Material and S3 Fig. We also conducted a global sensitivity analysis by running a Latin Hypercube Sampling and calculating the Pearson's Correlation Coefficient (PCC) for each parameter with the final tumour size. Other sensitivity analysis methods, such as eFAST, MeFAST or Sobol, would also have been appropriate here [73].

In silico clinical trial

Virtual clinical trials (VCT), also known as virtual patient cohorts, phase i trials, digital twins, and *in silico* clinical trials attempt to integrate the heterogeneity of actual patient responses and preclinical studies through a cohort of virtual patients or individuals [33,38–44,74].

Virtual patient generation from *in vivo* data. There are many ways to generate virtual patients [41,45,46] and in this work, we created virtual cohorts using two different methods employed by previous works [41,44,45]. We first created a cohort of patients that matched individual *in vivo* mouse tumour growth trajectories using acceptance-rejection sampling (Fig 3: Method (1)). We sampled 250,000,000 parameter sets $\theta = k, \epsilon, d_B, d_T, s, \eta, \beta$ from uniform distributions centered around the fitted parameter $\hat{p}$ values with bounds [0.001, 5]. We took the 400 parameter sets that gave the minimum residual to the individual tumour volume measurements, labelled "m1" to "m8". The second method we used to generate a virtual cohort, was a similar approach to that developed by Kim *et al.* [44]. We converted the change from baseline measurements for the clinical trial data to a probability density function (PDF) for the final tumour size x (Fig 3: Method (2)). We then sampled 400 patients from this PDF and optimised the set of

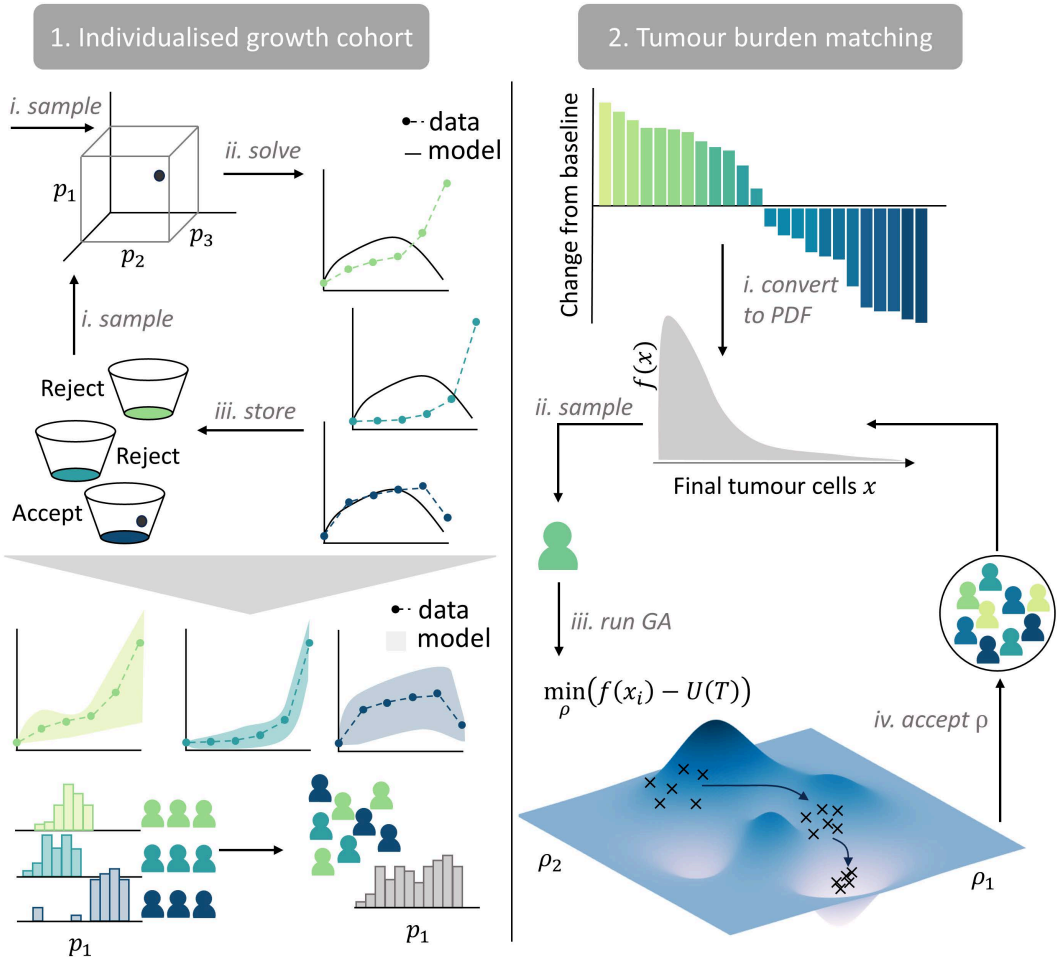

Fig 3. Illustration of the two virtual clinical trial generation methods: Method (1) individualised growth cohort and Method (2) tumour burden matching. Method (1) investigates heterogeneity arising in the *in vivo* measurements by matching the model to individual mouse tumour growth trajectories. Parameters are sampled from uniform multi-dimensional parameter distributions, and an acceptance-rejection algorithm is implemented, accepting samples that align closest with the data. Once a cohort of N samples for each individual tumour growth trajectory have been sampled, the distribution for these parameters, e.g., p_1, can be compared across the different trajectories. Method (2) generates the virtual cohort through converting measurements from a clinical trial measuring the change from baseline (CFB) to a probability density function (PDF) $f(x)$ for the final tumour size x. From this PDF, N individual final tumour sizes are sampled and a genetic algorithm is used to determine the optimal parameter combination for the model to match the CFB (%) data.

https://doi.org/10.1371/journal.pcbi.1014533.g003

parameters to obtain an estimate for the final model size that matched the sampled patient using a genetic algorithm (MATLAB's *ga*). This gave us a distribution of final tumour sizes and corresponding parameter values that matched the PDF obtained from the clinical data.

Virtual patient generation from Phase II clinical trial. In the Phase II T-VEC clinical trial, patients were required to have melanoma lesions appropriate for intralesional injection, defined as ≥ 1 lesion with a diameter of ≥ 10 mm or multiple lesions with a combined diameter of ≥ 10mm. Previous work by Dessinioti *et al.* [75] reported a median melanoma diameter of 13mm, with quartiles 9–20mm, and 10.6% of tumours below 6mm. Using these statistical summaries, we parameterised a gamma distribution and obtained a shape and scale parameter of 3.09 and 4.91 respectively (see Supplementary Information). To convert from tumour diameter to cell count, we assumed a spherical tumour volume, which gives $1,150.35\text{mm}^3$. We then assumed that $1\text{mm}^3 = 10^6$ cells which hl, for an initial tumour diameter of 13mm, gives an initial cell count of $U(0) = 1.15 \times 10^9$ cells. For the first virtual cohort investigation of the clinical trial measurements, we sampled 400 tumour diameters from the parameterised gamma distribution and converted them to cell counts which were used as initial conditions for the model. Following this, we fixed the initial cell count to the median tumour diameter, i.e., 13mm, and obtain virtual patients using Method (2) described above.

At baseline, the mean intratumoural CD8 + T cell density was 460 cells/mm^2 (range 5–3,963) for patients in the clinical trial [67]. If we assume the measurements were taken on 20μm samples, then this would give the approximate density of T cells in a 1mm^3 sample to be 4.6×10^4 cells/mm^3. As both L and η have cells as units and were estimated *in vivo* these were rescaled to a human context using the new initial number of tumour cells, see the Supplementary Information for explicit calculations. We have chosen to evaluate all patients at an equivalent final time to $T = 23$ weeks, as all treatments were continued for at least 6 months (unless they were not tolerated by the patient) [67]. To confirm the distribution for the change from baseline of the Phase II clinical trial cohort matched the virtual cohort, we used a Kolmogorov-Smirnov test for similarity using Matlab's function *kstest2*.

Results

Parameterisation and sensitivity of a mathematical representation for MV-BiTEs

To calibrate the model, we fit parameters from the system of ODEs in Eqs. 1–5 to *in vitro* measurements for viral progeny and cell viability (S1 Fig), and specific lysis (S2 Fig). We assumed the viral infectivity and CD3$^+$ T cell killing rate may vary *in vivo* and refit these using the *in vivo* tumour volume experiments (Fig 4A – 4E). Estimates for parameters can be found in Table 2 with more details in the Materials and Methods and Supplementary Information S1 Text. Qualitatively, we observed good agreement between the data and the model, supported by goodness of fit statistics, Table 3. To investigate the sensitivity of the parameterised model, we conducted a local (S3 Fig) and global (Fig 4F) parameter sensitivity analysis. The global sensitivity analysis suggested the immune-related parameters k, ϵ, and s had a negative correlation with the tumour size.

Table 3. Goodness of fit statistics for model fit to the data in Fig 4, with parameter values in Table 2.

Experiment	Figure	R-square	Residual
in vivo control	Fig 4D	0.9988	1.84×10^3
in vivo BiTEs	Fig 4E	0.9892	1.06×10^4
in vivo MV	Fig 4F	0.9466	4.22×10^4
in vivo MV-BiTE	Fig 4G	0.9968	1.27×10^4

https://doi.org/10.1371/journal.pcbi.1014533.t003

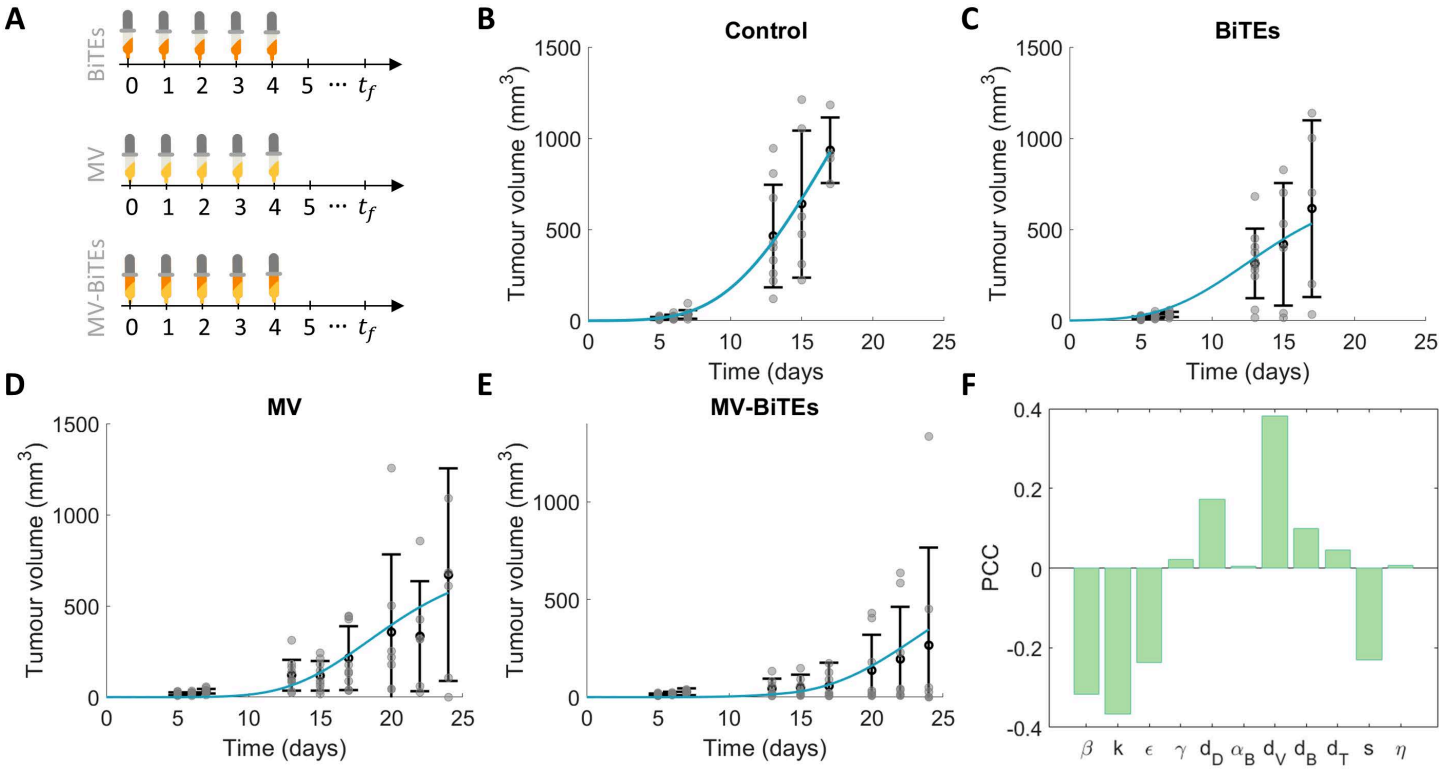

Fig 4. Parameterisation of the model for MV-BiTEs using *in vitro* and *in vivo* experiments. Generation of data is described in the Methods. (A) Experimental protocol for *in vivo* experiments with BiTEs, MV and MV-BiTEs. (B)-(E) Tumour volume *in vivo* in (B) control (mock) and (C) BiTEs only, (D) MV only and (E) MV-BiTEs treatment groups. Black circles with error bars are representative of the mean and standard deviation of the data and grey circles are individual data points. Solid blue lines represent the model's approximation to the data. (F) Pearson Correlation Coefficient (PCC) for a Latin Hypercube Sampling on [0.01, 2] capturing the sensitivity of the estimated parameters.

https://doi.org/10.1371/journal.pcbi.1014533.g004

Capturing inherent *in vivo* variability in tumour responses

In the *in vivo* experiment, mice exhibited heterogeneous responses to MV-BiTE treatment, with some mice experiencing tumour progression and others experiencing regression (Fig 5). To examine the model's ability to capture this heterogeneity, we sampled a virtual cohort using Method (1) (Fig 3) for each individual mouse, m1-m8. We obtained 400 parameter sets for each m1-m8 trajectory that gave the smallest residual to the data (Fig 5A – 5I, with example trajectories in S4 Fig). The model was able to capture the heterogeneous range of tumour growths exhibited by the mice upon MV-BiTE treatment.

Variability between the tumour growths is captured by the relative mean and standard deviation for each parameter (Fig 5J, with full distributions in S5 Fig). Noticeable differences in the mean for β exist, suggesting that virus administration is largely driving the heterogeneous responses in the mice. Furthermore, changes in ϵ and d_B seem to correlate with either tumour growth (m2, m3, and m7) or tumour decline (m1, m4-m6). This suggests that tumour growth or decline could be linked to the efficacy of CD3$^+$ T cells and the pharmacokinetics of BiTEs.

Examining correlations between parameters, we found that all individual growths, except m2, had a positive correlation between viral characteristics, η and β (S6 Fig), i.e., increasing one of these parameters resulted in an increase of the other. Furthermore, m2 - m6 all had a negative correlation between k and ϵ, i.e., increases in one parameter observed a decrease in the other. This suggests a link between viral parameters η and β, immune parameters k and ϵ, and the response to MV-BiTEs.

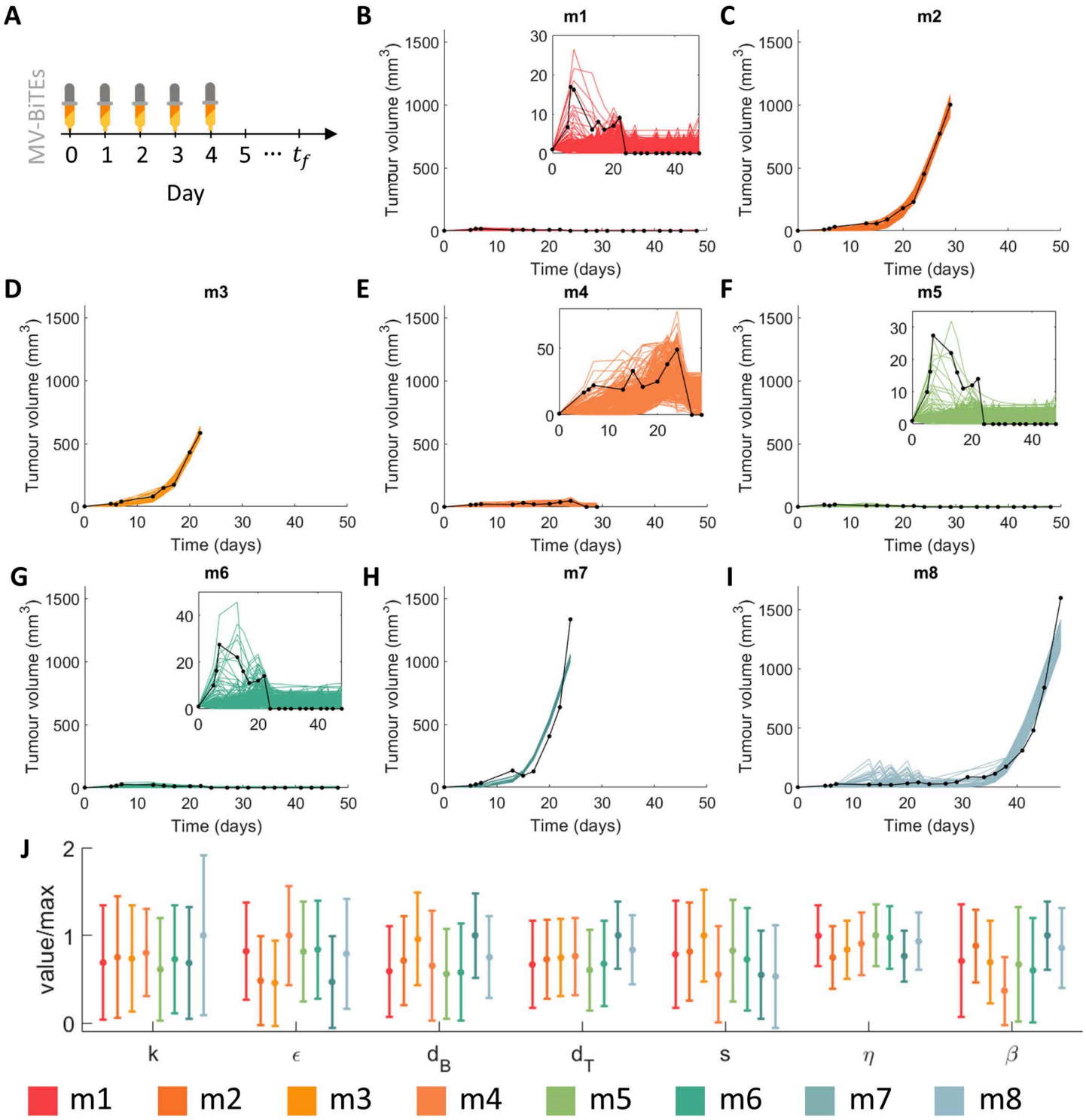

Fig 5. Obtaining model trajectories that match the tumour volume experimental measurements under the treatment schedule in (A). In the experiments, the tumour volume of 8 mice was tracked after treatment with MV-BiTEs with m1 to m8 in (B)-(I). The measurements for the mice are plotted on the same axis and represented by black dots, while the trajectories of the 400 parameter values sampled that gave the lowest residual error are plotted as coloured lines. Zoomed in inserts are provided when the trajectories are hard to visualise on the fixed axis. (J) The mean and standard deviation of the relative value for the parameters for each m1 to m8 are given as an error bar plot. These parameter ranges have been scaled relative to the maximum so they can be seen on the same figure. The corresponding parameter values and pair-wise correlations can be seen in the S4 and S6 Figs.

https://doi.org/10.1371/journal.pcbi.1014533.g005

Clustering individual responses into growth, delayed growth and remission

The responses to MV-BiTEs treatment can be grouped into three cohorts: 1. regression (m1, m4, m5, m6), 2. growth (m2, m3, m7,) and 3. delayed growth (m8). We generated data for these three virtual cohorts by sampling 400 parameter sets equally split amongst the mice belonging to that cohort (Fig 6A – 6C). Clear separation between the response cohorts can be seen in the final tumour size on day 48 (the final measurement across m1-m8) (Fig 6D). Not all trajectories in the growth cohort (cohort 2) are expected to surpass the delayed growth cohort, with some exhibiting small tumour sizes at

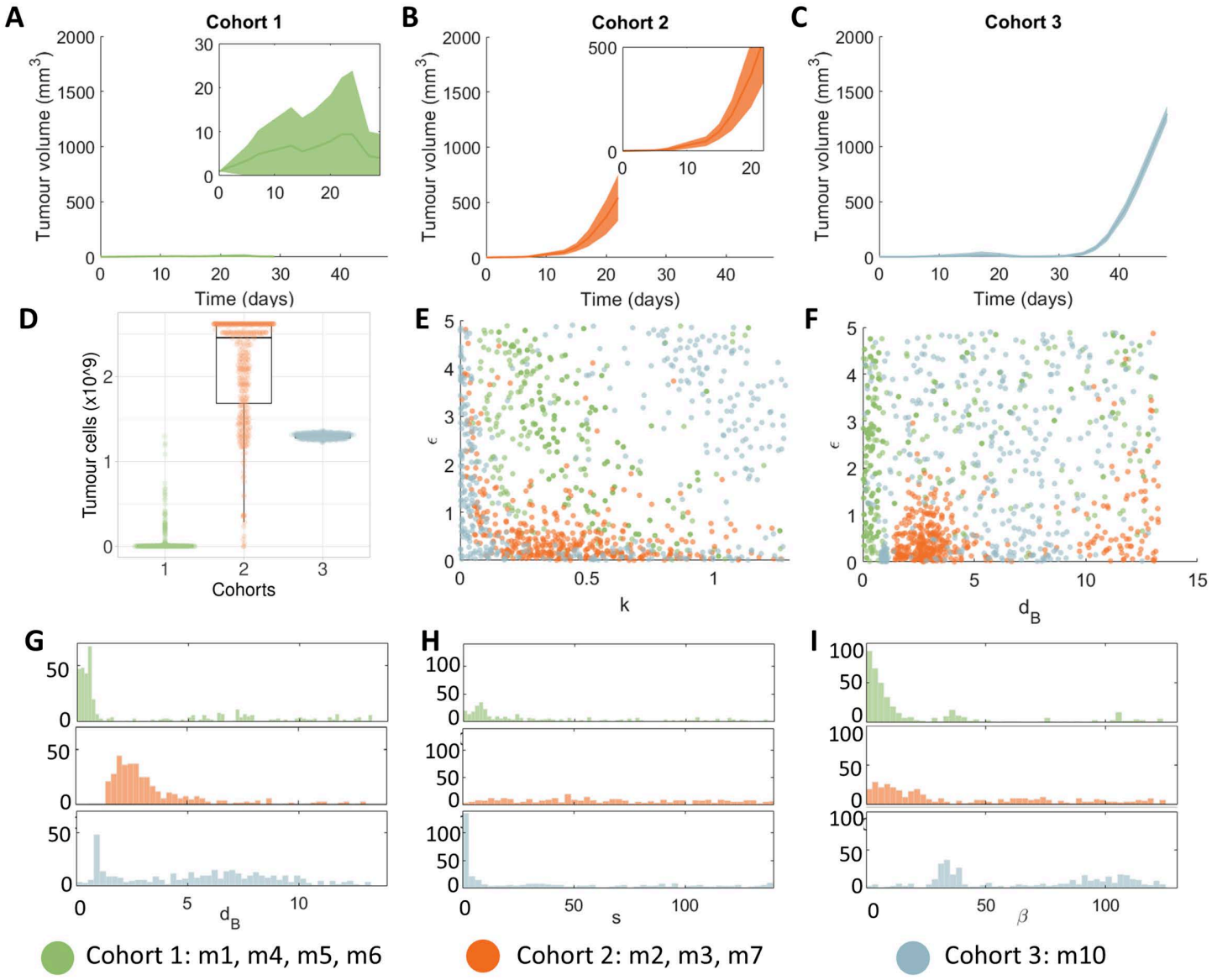

Fig 6. Analysing cohort characteristics. From the mice in Fig 5, three sub-cohorts were generated based on the dynamics in the data: regression (cohort 1), growth (cohort 2), delayed growth (cohort 3). (A-C) Mean tumour volumes and standard deviations for the three cohort values. (D) Final tumour cell number (as calculated for day 48) for each cohort. (E-F) For the three cohorts, the patterns within the parameter values are presented using scatter plots for ϵ vs k and d_B vs ϵ. Points are coloured based on the cohort. (G-I) Histograms for the parameters d_B, s, and β.

https://doi.org/10.1371/journal.pcbi.1014533.g006

day 48. This suggests that while the delayed growth cohort may at first seem to fare better compared to the growth cohort, some favourable trajectories are expected in the growth cohort.

Examining correlations between model parameters across the cohort we see distinctions in the clustering patterns for k and ϵ (Fig 6E). This suggests that the relationship between the killing rate and the basal killing efficacy are driving the response to MV-BiTE: low basal killing efficacy (ϵ) drives the growth cohort (cohort 2) and higher ratios of basal killing efficacy, and killing rates, drive the recovery cohort (cohort 1). Interestingly, there seems to be a bimodal relationship between these two parameters for the delayed growth cohort (cohort 3) suggesting that there are two possible explanations for tumour growth in this cohort. Similarly, there is clustering in the relationship between d_B and ϵ (Fig 6F), whereby for small basal killing efficacy and values of BiTE clearance, d_B, between 2 and 7 gives rise to the growth cohort (cohort 2). Comparing single parameter distributions (Fig 6G – 6I) the regression cohort (cohort 1) has very low d_B and β and the growth cohort (cohort 2) has very low β but slightly higher d_B, suggesting again that BiTE clearance is a key determinant of the response to MV-BiTEs.

Efficacy of administration protocol on variable tumour growths

For the three response cohorts (regression, growth, and delayed growth), we next investigated the effect of varying the MV-BiTEs administration protocol. We varied the number of dosages, n, and days between dosages, τ (Fig 7A) with the total virus dose kept constant. Variations to the MV-BiTEs protocol had a negligible effect on the regression cohort (cohort 1) (Fig 7B (top row) and S7 Fig), suggesting this cohort will always respond to MV-BiTEs irrespective of the administration protocol. A larger dependence on the protocol is seen for the growth cohort (cohort 2) and delayed growth cohort (cohort 3). The optimal protocol for these cohorts is more injections given further apart.

Taking the optimal protocol to be 7 injections 6 days apart, we found that there is clear separation between the best and worst responses in the growth (cohort 2) and delayed growth (cohort 3) cohorts. For instance, in cohort 2, there is a clear separation in the pair-wise relationships between d_B and β, and d_B and k, respectively (Fig 7C – 7D). This suggests that we can determine individuals who will respond best to this treatment protocol based on their BiTE pharmacokinetics, viral infectivity and CD3 killing rates. Similarly, in the delayed growth cohort (cohort 3) (Fig 7E) individuals who respond best have high CD3 killing and basal kill rates. We then examined whether this optimal protocol holds under the condition that after treatment ends, we resect the tumour 7 days later (Fig 8B (bottom row)). In this scenario, all protocols are similar as 7 days after treatment, the model predicts all cohorts are responding to MV-BiTEs. The rationale behind this metric is that it helps to evaluate the efficacy of treatment in controlling tumour growth by examining the impact once the treatment is halted and the tumour has time to regrow.

Case study: Virtual cohort representative of human responses

To examine the robustness of our model and its predictions for a clinical setting, we generated a virtual cohort using the Phase II clinical trial of T-VEC [67]. As no in-human data of MV-BiTEs therapy exists, we used a study of an advanced oncolytic virus encoding an immunostimulatory agent as a surrogate, here a herpes simplex type 1-derived OV encoding GM-CSF, as a surrogate. Melanoma was the targeted tumour entity in both the pre-clinical MV-BiTEs study and the T-VEC trial. In this clinical trial, an intratumoural injection of $V_{d1} = 10^6$ was administered initially, followed by fortnightly booster injections of $V_{d2} = 10^8$ starting 3 weeks after the initial T-VEC injection. The percentage change from baseline (CFB) for 98 patients was then recorded (Fig 8A). We assumed the same dosage size for MV-BiTEs as used for T-VEC in the clinical trial and included the addition of BiTEs in the injection to match our *in vivo* experiments. We fixed the final time of the simulation as $T = 23$ weeks ($T = 161$ days) and measured the resulting tumour size $U(T)=U(161)$.

We first examined whether heterogeneity in the initial tumour burden could explain the change from baseline (CFB) measurements in the clinical trial. To do this, we parameterised a gamma distribution using summary statistics reported by Dessinioti *et al.* [75] for the diameter of melanomas in 537 cases (see Methods and Supplementary Information for

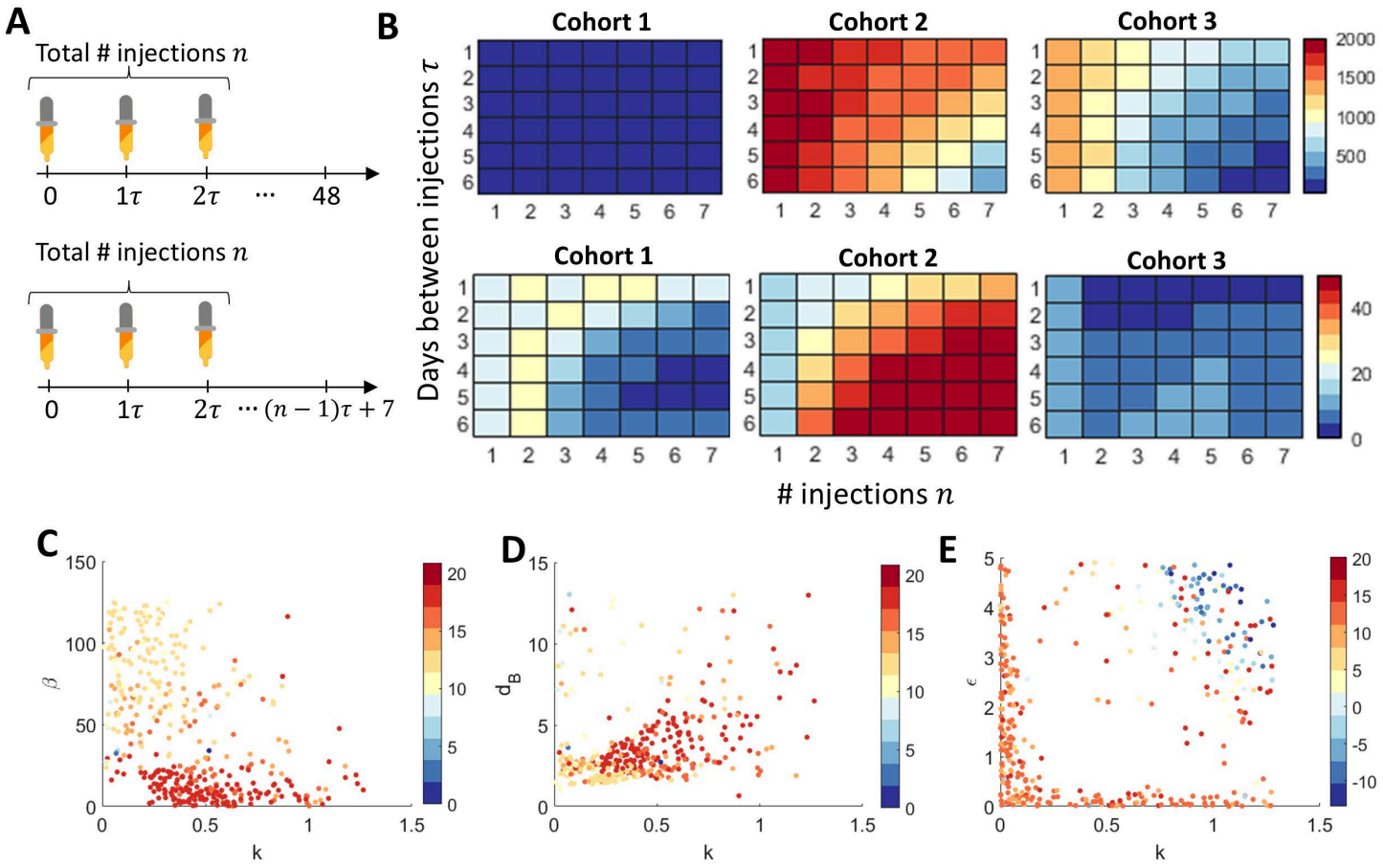

Fig 7. The impact of the treatment protocol on the three cohort responses: 1) regression, 2) growth, and 3) delayed growth. (A) Treatment protocols considered varied the number of injections n and days between injections τ. (B) The effect of the protocol on the mean tumour size (in mm3) for each cohort at either 48 days (top row) or 7 days after the final injection (bottom row). (C-D) Parameter correlations for cohort 2: (C) *k* vs β and (D) *k* vs d_B. (E) Parameter correlations for cohort 3 for *k* vs ϵ. All scatter plots are based on 7 injections given 6 days apart with parameter pairs represented as points coloured by the log tumour size at 48 days.

https://doi.org/10.1371/journal.pcbi.1014533.g007

details). We then sampled 400 virtual patient initial tumour diameters (Fig 8B) and converted these to initial cell counts to feed into the model. The resulting CFB predicted from the model for heterogeneous initial tumour sizes was unable to capture the range of the clinical trial measurements (Fig 8C). This suggests that changes to parameters, representing patient-specific characteristics, are needed to capture clinical outcomes.

We next chose to follow Method (2), (Fig 3) to generate a cohort of 400 virtual patients (Method (2), Fig 3). We sampled 400 CFB to create a larger sample of human patients and ran a genetic algorithm to determine optimal parameter sets that matched the sampled CFB (S8 Fig). We fixed the initial tumour size to the median melanoma diameter and chose three parameters to optimise, k, d_B, and r (Fig 8D), based on their sensitivity so far revealed in our analysis. The genetic algorithm returned a close match between individual virtual patient samples and the model (Fig 8E – 8F). The distributions for the change from baseline of the real patient cohort and virtual patient cohort qualitatively match and passed the Kolmogorov-Smirnov test for similarity. We then examined the correlations between patient parameters and their resulting change from baseline (Fig 8D, with all correlations in S8 Fig). We found a particularly strong correlation between the tumour growth rate, *r*, and the T cell killing rate, *k*, with low growth rates and strong immune responses showing the

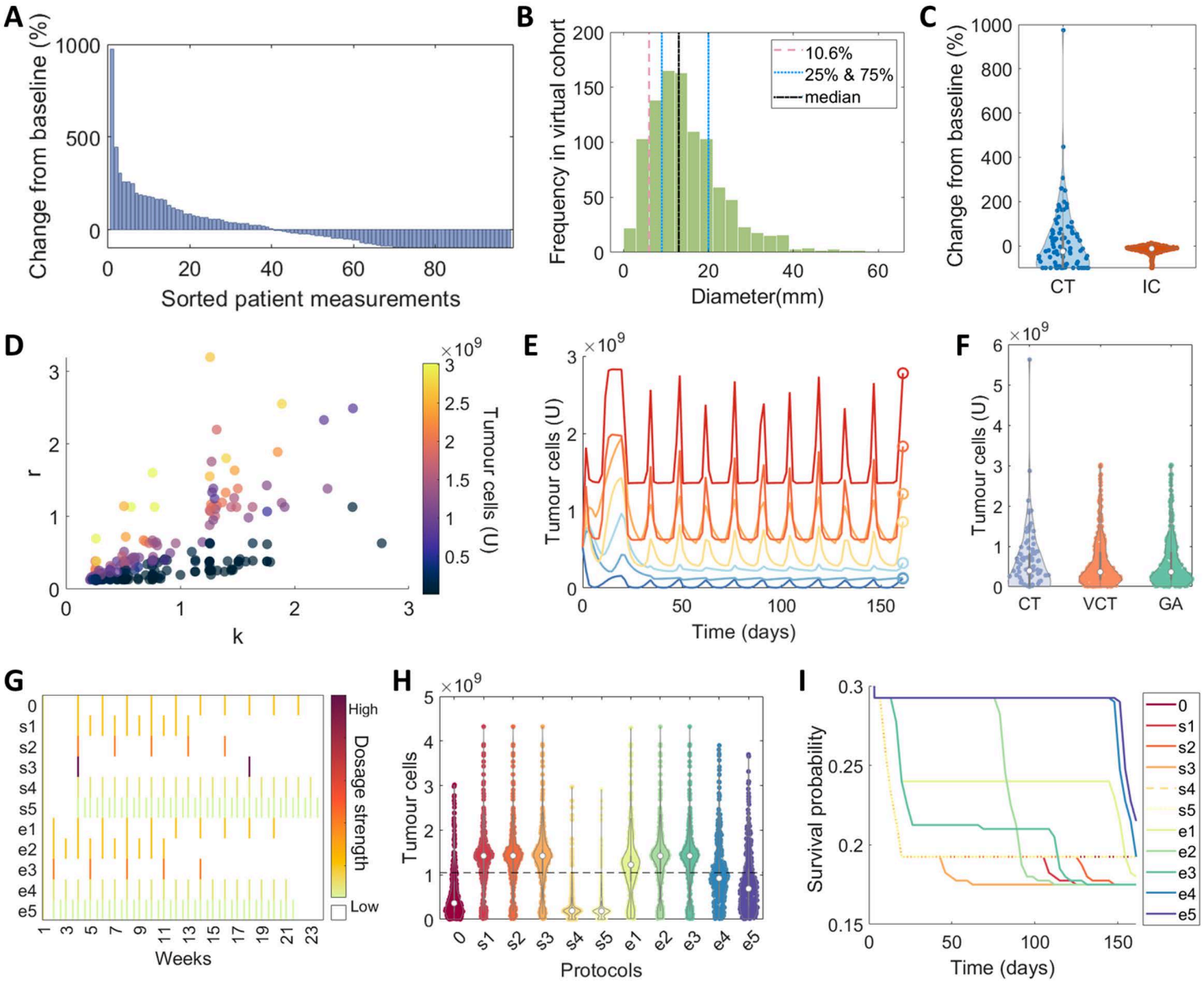

Fig 8. Expanding a virtual patient cohort informed by the Phase II T-VEC clinical trial [67]. (A) Change from baseline (%) for the Phase II T-VEC clinical trial digitized using WebPlotDigitiser [76]. (B) Distribution of initial tumour diameters for 400 virtual patients sampled from a gamma distribution estimated from the summary statistics of Dessinioti *et al.* [75] overlaid as vertical lines: 10.6% (dashed orange), 25% and 75% (blue dotted), and median (black dot dash). (C) Violin plots comparing the change from baseline for the clinical trial (CT) measurements and model simulations from the sampled initial tumour diameters (IC). (D) Scatter plot for parameters r vs k obtained from optimising the model output to the CT measurements using a genetic algorithm, i.e., Method (2). Each disk represents a patient with the colour representing the tumour cell count. (E) Plot showing the agreement between the model (solid lines) and patient samples (open circles) for 7 virtual patients (colour matched). (F) The distribution for the total number of tumour cells predicted by the model at T = 23 weeks and those in the CT, the samples for the 400 virtual patients (VCT), and model predictions using a genetic algorithm (GA).(G) Summary of the original clinical trial dosage protocol and the 10 hypothetical protocols considered (Table 4). Coloured bars represent the strength of a dosage given in a particular week. (H) The final tumour cell counts for varying treatment protocols examined (s1-s5, e1-e5) compared to the original protocol 0. (I) Kaplan-Meier survival curves corresponding to (E) for a threshold of a 120% CFB. Note the survival probability range is plotted on [0.15 to 0.3].

https://doi.org/10.1371/journal.pcbi.1014533.g008

Table 4. Summary of the standard clinical trial protocol and the 10 hypothetical protocols examined in Fig 8. Note that the frequency and total doses are given from the booster dose onwards.

Label	Booster	Frequency	Total doses
	standard = 3 weeks, early = 1 week		
0	standard	3 weekly	10
s1	standard	1 week	10
s2	standard	3 weeks	5
s3	standard	14 weeks	2
s4	standard	1 week	30
s5	standard	3.5 days	40
e1	early	2 weeks	10
e2	early	1 week	10
e3	early	3 weeks	5
e4	early	1 week	20
e5	early	3.5 days	40

https://doi.org/10.1371/journal.pcbi.1014533.t004

largest negative CFB. The clearance of BiTEs, d_B, also seems to positively correlate with CFB suggesting that a faster clearance of BiTEs results in a larger tumour size.

Case study: Impact of alternate treatment protocols on *in silico* human clinical trial

Lastly, we chose to examine whether an alternate, more effective, protocol exists. We generated 10 hypothetical treatment protocols that examined either the standard booster onset time (i.e., 3 weeks following the first V_{d1} dose) or an earlier booster onset time (i.e., 1 week following the first V_{d1} dose) and then varying intervals between V_{d2} doses and their multiplicity (Table 4 and Fig 8G). The total administered dose of MV-BiTEs, i.e., $V_{TOT} = 20 \times V_{d2}$ was fixed across all protocols considered. Reduction in tumour size was largest under the standard booster onset (3 weeks after the first injection) with more injections given more regularly (s4 and s5, Fig 8H). In contrast, intervals between consecutive doses larger than the current standard fortnightly protocol, do not improve the average tumour burden (i.e., s1-s3, e1-e3). To examine the relationship between final tumour size and hypothetical survival curves for our virtual cohort, we have plotted the Kaplan-Meier survival curves under the 10 protocols for a survival threshold of 120% CFB (Fig 8I). These suggest that individuals predicted to have large tumour sizes early on under the standard protocol will benefit in the short-term from the early booster onset protocols with frequent smaller dosages (e4 and e5).

Discussion

The potential therapeutic efficacy of BiTEs delivered by oncolytic viral vectors is an exciting area of immunotherapy. In this work, we develop a mathematical platform that can be used to simulate the efficacy of this novel therapeutic strategy. We show how this model recapitulates the dynamics of MV-BiTE *in vitro* and *in vivo*, as well as matches change from baseline (%) measurements in a Phase II clinical trial for T-VEC. Generating *in silico* clinical trials, we unravel the likely mechanistic drivers of the heterogeneity in responses to MV-BiTEs as well as propose potentially more effective protocols. This hypothesis-generating platform serves to better inform future experiments and, hopefully, the translation into clinical trials.

An overarching theme of this research has been to understand the impact of alterations to the MV-BiTEs administration protocol. Mathematical modelling is especially valuable to address this question, since it would be impossible (and unethical) to systemically test all conceivable perturbations in animal experiments. With our predictions, we can prioritise certain protocols for *in vivo* validation.

Despite good alignment of the model with our experimental data and despite delivering insightful simulations, this study has some limitations. Importantly, we do not expect MV-BiTEs therapy to yield the same results in a clinical trial as those in the Phase II T-VEC trial and instead use the results of this clinical trial as an example of heterogeneity that may be seen in an MV-BiTEs protocol. In the future, clinical data might be obtained from studies on BiTE-encoding OVs that more closely recapitulate the interactions described by the ODEs developed in this work. One such example is an ongoing clinical trial investigating an oncolytic adenovirus encoding several immunomodulatory transgenes including a FAP-targeting T cell engager [NCT04053283, [77]; NCT05043714, [78]]. Another caveat is the low number of individual mice the cohort simulation is based on, especially for the delayed tumour growth cohort 3 (n = 1). Additional *in vivo* studies are expected to generate a more robust basis for our simulations, while dedicated measurements of, e.g., phagocytosis and antigen presentation can help to dissect additional aspects of immunological responses to OV-BiTEs therapy.

We found consistently throughout our simulations that lower-dosage injections given more frequently were predicted to reduce the tumour size most significantly. In both the *in silico* clinical trials based on the *in vivo* tumour growth and the Phase II clinical trial data, we saw that more frequent injections were optimal. Furthermore, we found that an initial dosage followed by a short delay in the following booster dosage (3 weeks) followed by frequent small doses was most effective. This suggests that once the treatment effect has time to establish after the first dosage, frequent small dosages are more effective than large bolus dosages given far apart. However, in experimental and clinical practice, this might pose a challenge due to tumour growth in the intervals between injections and, therefore, needs to be carefully evaluated in a well-designed animal experiment beforehand. Another caveat to this is that our model predicted individuals who would respond to MV-BiTE, would likely respond irrespective of the administration protocol. By contrast, those classified as experiencing tumour "growth" or having a large change from baseline (%) would benefit most from a change in protocol. This suggests that if it were possible to pre-determine which classification an individual patient would fall into, it would be possible to predict their potential success under treatment with MV-BiTEs.

In both *in silico* clinical trials generated, $CD3^+$ T cell cytotoxicity and BiTE pharmacokinetic clearance were predicted to determine whether the tumour regressed or grew. This is in line with previous clinical findings that identified pre-existing T cell responses towards measles virus and tumour antigens to correlate with outcome of MV therapy [79]. *In vivo* experiments [13] as well as the mathematical model showed that encoding BiTEs in the MV vector is crucial for therapeutic effectiveness as compared to direct BiTE injections. Nevertheless, simulations indicated that a high BiTE clearance rate limited therapeutic success. This points towards temporary BiTE effects despite vector-mediated expression. Differences in BiTE pharmacokinetics could be due to individual immune responses (e.g., via neutralising antibodies or phagocytosis), variations in tumour composition (e.g., areas of hyperproliferation, hypoxia, or necrosis), or restrictions in the tumour microenvironment such as dense stroma. Predicting potentially crucial parameters may prove helpful in the search for biomarkers of response. If candidate parameters could be measured prior to treatment onset, e.g., levels of neutralising antibodies, they can be correlated with the predicted treatment outcome for validation. If this holds true, stratification into biomarker-adapted treatment arms could improve overall outcome.

In addition, our findings suggest that targeting BiTE pharmacokinetics could be one next avenue forward for experimental design, e.g., testing other, potentially more stable protein formats that have been proposed, such as DARTs, diabodies, or IgG-like structures [80, 81]. In addition, alternative vectors have been considered for delivery of BiTEs, such as other OVs [12,15], (CAR) T cells [82,83], or nanocarriers that deliver *in vitro*-transcribed mRNA encoding BiTEs to host myeloid cells [84]. Comparing the pharmacokinetics of these vectors could lead to improved efficacy at the clinical level. Importantly, our findings in patient-derived xenograft models with tumour cells of human origin showed extended BiTE expression compared to the murine tumour model, indicating that limited MV-BiTE effectiveness can, at least in part, be attributed to restricted viral replication in murine cells [13], giving hope for better outcomes in human patients.

There are certain limitations in our model based on some simplifying assumptions. For example, we assumed the growth of the control cell population in the cell viability measurements was negligible (see Supplementary Material). The growth of

the cells *in vitro* would have likely been highly non-linear with periods of growth, saturation and then decline. Future work will investigate this limitation further by generating data for the cell viability measurements that may be used to better calibrate the model. We are confident, however, that the model still provides a sufficient baseline for approximating the impact of viral infection and death of tumour cells as a large number of parameters were recalibrated to the *in vivo* data.

Furthermore, a wide range of biological processes is involved in anti-tumour T cell effects, including activation via the endogenous T cell receptor and/or bispecific T cell engagers, replication of individual T cell clones, stimulation and inhibition by cytokines and other mechanisms, and T cell exhaustion. While our model captures rates of T cell accumulation, decay, and baseline as well as BiTE-induced tumor cell killing, it does not explicitly account for T cell exhaustion, which is a common mechanism found in cancer and, more specifically, in both OV and BiTE therapies. Various concepts such as OV-encoded immune checkpoint inhibitors or BiTE treatment-free intervals have been devised to address this [85–88]. In a future version of the model, we aim to implement T cell exhaustion on the basis of time-resolved functional T cell characterisation to better reflect cases of treatment failure under continuous BiTE release by OV-infected cells. This can subsequently be used to predict optimal combination or dosing strategies for long-term anti-tumour efficacy with specific focus on functional exhaustion of T cells.

In addition, MV-BiTEs can form syncytia which is omitted from our model. With the addition of data quantifying the presence of syncytia, we could extend the model to capture the effect of this on viral spread as is done in other mathematical models [89,90].

Taken together, our model serves as a platform for future research in OV-BiTEs to be conducted and hypotheses to be tested. In particular, testing of more stable bispecific protein formats and investigation of selected treatment protocols will be conducted as experimental validation. Such validation is crucial for any modelling prediction. Thereby, we aim at refining the model using novel datasets and, ultimately, at further developing complex combination immunovirotherapies towards clinical translation.

Supporting information

S1 Text. Details on the parameter fitting, parameter sensitivity and supporting analysis of the virtual cohort parameters.
(PDF)

S1 Fig. Model simulation of the fit to cell viability and viral progeny measurements from B16 cells using Eq. S1. The fits (solid lines) for (A) cell viability and (B) viral progeny, are shown against the individual experiment measurements (circle). Note in (B) the same fit is presented on a linear (left) and log (right) plot.
(TIF)

S2 Fig. Fitting data from LDH release assay to obtain an estimate for BiTE-mediated tumour cell killing by T cells, i.e., ϵ, k and γ. The mean and standard deviation for specific lysis % for varying BiTE concentrations is plotted in black. The model approximation using Eq. S2 is plotted in blue.
(TIF)

S3 Fig. Local pair-wise parameter perturbation by $\hat{p}$ giving the relative total tumour cells on day 25 (Eq. S3) is represented by the colour bar. Direction of perturbation is increasing moving down vertically and across horizontally for each parameter value.
(TIF)

S4 Fig. Four individual parameter sets and their resulting model trajectories against m4's data. These four-exemplar parameter sets, and their model trajectories are a subset of those plotted on Fig 5. The black line and solid circles are the tumour volume measurements, and the orange curve is the model's predicted solution.
(TIF)

S5 Fig. Sampled parameters that give model trajectories matching the data for individual mice m1-m8 (Method (1), Fig 3). Sampled 250,000,000 parameter sets and calculated the residual to each of the 8 mice's tumour volume, i.e., m1 through to m8. The 400 parameter sets giving the lowest residual have been plotted as histograms for $k, \epsilon, d_B, d_T, s, \eta$ and β with their trajectories against the data of individual mice, mean values and standard deviations in Fig 5.
(TIF)

S6 Fig. Pairwise scatter plots for significant parameter correlations across the 8 mice, m1-m8. The *x*,*y* labels denote the parameters of interest, and the titles denote the mouse. Points correspond to the specific parameter values for that mouse. The colour of points corresponds to the mouse.
(TIF)

S7 Fig. Impact of the number of injections and days between injections of MV-BiTEs for the three cohorts: 1) recovery, growth and delayed-growth, corresponding to Fig 7. The corresponding mean and standard deviation for the three cohorts (c1, c2, and c3) at (A-B) 48 days and (C-D) 7 days after the last injection.
(TIF)

S8 Fig. Additional information about the virtual cohort expanded from human clinical trial data. (A) Change from baseline (%) for the Phase II T-VEC clinical trial digitized using WebPlotDigitiser. (B) Probability density function (PDF) generated for the clinical trial data and compared to the virtual clinical trial (VCT) samples. (C) The resulting change from baseline for the model's optimised parameters using a genetic algorithm. (D) Correlation matrix for the three patient-specific parameters sampled to match the final tumour size of the virtual patients $U(T)$.
(TIF)

Author contributions

Conceptualization: Adrianne L. Jenner, Christine E. Engeland, Johannes P. W. Heidbuechel.

Data curation: Christine E. Engeland, Johannes P. W. Heidbuechel.

Formal analysis: Adrianne L. Jenner, Noa L. Levi.

Investigation: Adrianne L. Jenner, Christine E. Engeland, Johannes P. W. Heidbuechel.

Methodology: Robyn P. Araujo.

Resources: Guy Ungerechts, Christine E. Engeland, Johannes P. W. Heidbuechel.

Visualization: Adrianne L. Jenner.

Writing – original draft: Adrianne L. Jenner, Noa L. Levi, Johannes P. W. Heidbuechel.

Writing – review & editing: Robyn P. Araujo, Guy Ungerechts, Christine E. Engeland, Johannes P. W. Heidbuechel.

References

1. Esfahani K, Roudaia L, Buhlaiga N, Del Rincon SV, Papneja N, Miller WH Jr. A review of cancer immunotherapy: from the past, to the present, to the future. Curr Oncol. 2020;27(Suppl 2):S87–97. https://doi.org/10.3747/co.27.5223 PMID: 32368178
2. Huehls AM, Coupet TA, Sentman CL. Bispecific T-cell engagers for cancer immunotherapy. Immunol Cell Biol. 2015;93(3):290–6. https://doi.org/10.1038/icb.2014.93 PMID: 25367186
3. Kamrani A, Nasiri H, Hassanzadeh A, Ahmadian Heris J, Mohammadinasab R, Sadeghvand S, et al. New immunotherapy approaches for colorectal cancer: focusing on CAR-T cell, BiTE, and oncolytic viruses. Cell Commun Signal. 2024;22(1):56. https://doi.org/10.1186/s12964-023-01430-8 PMID: 38243252
4. Tian Z, Liu M, Zhang Y, Wang X. Bispecific T cell engagers: an emerging therapy for management of hematologic malignancies. J Hematol Oncol. 2021;14(1):75. https://doi.org/10.1186/s13045-021-01084-4 PMID: 33941237
5. Ellerman D. Bispecific T-cell engagers: towards understanding variables influencing the in vitro potency and tumor selectivity and their modulation to enhance their efficacy and safety. Methods. 2019;154:102–17. https://doi.org/10.1016/j.ymeth.2018.10.026 PMID: 30395966

6. Maus MV, Grupp SA, Porter DL, June CH. Antibody-modified T cells: CARs take the front seat for hematologic malignancies. Blood. 2014;123(17):2625–35. https://doi.org/10.1182/blood-2013-11-492231 PMID: 24578504
7. Paulson KG, Lau SCM, Ahn M-J, Moskovitz M, Pogorzelski M, Häfliger S, et al. Safety and activity of tarlatamab in combination with a PD-L1 inhibitor as first-line maintenance therapy after chemo-immunotherapy in patients with extensive-stage small-cell lung cancer (DeLLphi-303): a multicentre, non-randomised, phase 1b study. Lancet Oncol. 2025;26(10):1300–11. https://doi.org/10.1016/S1470-2045(25)00480-2 PMID: 40934933
8. Mountzios G, Sun L, Cho BC, Demirci U, Baka S, Gümüş M, et al. Tarlatamab in small-cell lung cancer after platinum-based chemotherapy. N Engl J Med. 2025;393(4):349–61. https://doi.org/10.1056/NEJMoa2502099 PMID: 40454646
9. Stein MN, Vinceneux A, Robbrecht D, Doger B, Autio KA, Schweizer MT, et al. Pasritamig, a first-in-class, bispecific T-cell engager targeting human kallikrein 2, in metastatic castration-resistant prostate cancer: a phase I study. J Clin Oncol. 2025:JCO-25.
10. Chiang AC, Olmedo Garcia ME, Carlisle JW, Dowlati A, Reguart N, Felip E, et al. Safety of tarlatamab with 6-8-h outpatient versus 48-h inpatient monitoring during cycle 1: DeLLphi-300 phase 1 substudy. ESMO Open. 2025;10(4):104538. https://doi.org/10.1016/j.esmoop.2025.104538 PMID: 40187110
11. Lopez JS, Milhem M, Butler MO, Thistlethwaite F, Van Tine BA, D'Angelo SP, et al. Phase 1 study of IMCnyeso, a T cell receptor bispecific ImmTAC targeting NY-ESO-1-expressing malignancies. Cell Rep Med. 2025;6(4).
12. Heidbuechel JPW, Engeland CE. Oncolytic viruses encoding bispecific T cell engagers: a blueprint for emerging immunovirotherapies. J Hematol Oncol. 2021;14(1):63. https://doi.org/10.1186/s13045-021-01075-5 PMID: 33863363
13. Speck T, Heidbuechel JPW, Veinalde R, Jaeger D, von Kalle C, Ball CR, et al. Targeted BiTE expression by an oncolytic vector augments therapeutic efficacy against solid tumors. Clin Cancer Res. 2018;24(9):2128–37. https://doi.org/10.1158/1078-0432.CCR-17-2651 PMID: 29437789
14. Lei W, Ye Q, Hao Y, Chen J, Huang Y, Yang L, et al. CD19-targeted BiTE expression by an oncolytic vaccinia virus significantly augments therapeutic efficacy against B-cell lymphoma. Blood Cancer J. 2022;12(2):35. https://doi.org/10.1038/s41408-022-00634-4 PMID: 35228544
15. Kontermann RE, Ungerechts G, Nettelbeck DM. Viro-antibody therapy: engineering oncolytic viruses for genetic delivery of diverse antibody-based biotherapeutics. MAbs. 2021;13(1):1982447. https://doi.org/10.1080/19420862.2021.1982447 PMID: 34747345
16. Wang Y, Cheng P. Arming oncolytic viruses with bispecific T cell engagers: the evolution and current status. Biochim Biophys Acta Mol Basis Dis. 2024;1870(2):166962. https://doi.org/10.1016/j.bbadis.2023.166962 PMID: 37984801
17. Yu F, Wang X, Guo ZS, Bartlett DL, Gottschalk SM, Song X-T. T-cell engager-armed oncolytic vaccinia virus significantly enhances antitumor therapy. Mol Ther. 2014;22(1):102–11. https://doi.org/10.1038/mt.2013.240 PMID: 24135899
18. Fajardo CA, Guedan S, Rojas LA, Moreno R, Arias-Badia M, de Sostoa J, et al. Oncolytic adenoviral delivery of an EGFR-targeting T-cell engager improves antitumor efficacy. Cancer Res. 2017;77(8):2052–63. https://doi.org/10.1158/0008-5472.CAN-16-1708 PMID: 28143835
19. Freedman JD, Hagel J, Scott EM, Psallidas I, Gupta A, Spiers L, et al. Oncolytic adenovirus expressing bispecific antibody targets T-cell cytotoxicity in cancer biopsies. EMBO Mol Med. 2017;9(8):1067–87. https://doi.org/10.15252/emmm.201707567 PMID: 28634161
20. Enekegho L, Stuart D. Smart oncolytic adenovirotherapy to induce killing of cancer cells and elicit antitumor immunity. Eureka. 2022;7(1):1–18. https://doi.org/10.29173/eureka28752
21. Song X-T. Combination of virotherapy and T-cell therapy: arming oncolytic virus with T-cell engagers. Discov Med. 2013;16(90):261–6. PMID: 24333405
22. Scott EM, Duffy MR, Freedman JD, Fisher KD, Seymour LW. Solid tumor immunotherapy with T cell engager-armed oncolytic viruses. Macromol Biosci. 2018;18(1):10.1002/mabi.201700187. https://doi.org/10.1002/mabi.201700187 PMID: 28902983
23. Guo ZS, Lotze MT, Zhu Z, Storkus WJ, Song X-T. Bi- and tri-specific T cell engager-armed oncolytic viruses: next-generation cancer immunotherapy. Biomedicines. 2020;8(7):204. https://doi.org/10.3390/biomedicines8070204 PMID: 32664210
24. Engeland CE, Heidbuechel JPW, Araujo RP, Jenner AL. Improving immunovirotherapies: the intersection of mathematical modelling and experiments. ImmunoInformatics. 2022;6:100011. https://doi.org/10.1016/j.immuno.2022.100011
25. Victori P, Buffa FM. The many faces of mathematical modelling in oncology. Br J Radiol. 2019;92(1093):20180856. https://doi.org/10.1259/bjr.20180856 PMID: 30485129
26. Rockne RC, Hawkins-Daarud A, Swanson KR, Sluka JP, Glazier JA, Macklin P, et al. The 2019 mathematical oncology roadmap. Phys Biol. 2019;16(4):041005. https://doi.org/10.1088/1478-3975/ab1a09 PMID: 30991381
27. Heidbuechel JPW, Abate-Daga D, Engeland CE, Enderling H. Mathematical modeling of oncolytic virotherapy. In: Oncolytic viruses. Springer; 2020. p. 307–20. https://doi.org/10.1007/978-1-4939-9794-7_21
28. Mahasa KJ, Ouifki R, Eladdadi A, De Pillis L. A combination therapy of oncolytic viruses and chimeric antigen receptor T cells: a mathematical model proof-of-concept. Math Biosci Eng. 2022;19(5):4429–57. https://doi.org/10.3934/mbe.2022205 PMID: 35430822
29. Zheng CY, Kim PS. Mathematical model for delayed responses in immune checkpoint blockades. Bull Math Biol. 2021;83(10):106. https://doi.org/10.1007/s11538-021-00933-0 PMID: 34477976
30. Pérez-García VM, León-Triana O, Rosa M, Pérez-Martínez A. CAR T cells for T-cell leukemias: insights from mathematical models. CNSNS. 2021;96:105684. https://doi.org/10.1016/j.cnsns.2020.105684
31. Gong C, Milberg O, Wang B, Vicini P, Narwal R, Roskos L, et al. A computational multiscale agent-based model for simulating spatio-temporal tumour immune response to PD1 and PDL1 inhibition. J R Soc Interface. 2017;14(134):20170320. https://doi.org/10.1098/rsif.2017.0320 PMID: 28931635

32. Ghaffari Laleh N, Loeffler CML, Grajek J, Staňková K, Pearson AT, Muti HS, et al. Classical mathematical models for prediction of response to chemotherapy and immunotherapy. PLoS Comput Biol. 2022;18(2):e1009822. https://doi.org/10.1371/journal.pcbi.1009822 PMID: 35120124
33. Cassidy T, Craig M. Determinants of combination GM-CSF immunotherapy and oncolytic virotherapy success identified through in silico treatment personalization. PLoS Comput Biol. 2019;15(11):e1007495. https://doi.org/10.1371/journal.pcbi.1007495 PMID: 31774808
34. Wares JR, Crivelli JJ, Yun C-O, Choi I-K, Gevertz JL, Kim PS. Treatment strategies for combining immunostimulatory oncolytic virus therapeutics with dendritic cell injections. Math Biosci Eng. 2015;12(6):1237–56. https://doi.org/10.3934/mbe.2015.12.1237 PMID: 26775859
35. Bajzer Z, Carr T, Josić K, Russell SJ, Dingli D. Modeling of cancer virotherapy with recombinant measles viruses. J Theor Biol. 2008;252(1):109–22. https://doi.org/10.1016/j.jtbi.2008.01.016 PMID: 18316099
36. Dingli D, Cascino MD, Josić K, Russell SJ, Bajzer Ž. Mathematical modeling of cancer radiovirotherapy. Math Biosci. 2006;199(1):55–78. https://doi.org/10.1016/j.mbs.2005.11.001
37. Van De Vyver A, Eigenmann M, Ovacik M, Pohl C, Herter S, Weinzierl T, et al. A novel approach for quantifying the pharmacological activity of T-cell engagers utilizing in vitro time course experiments and streamlined data analysis. AAPS J. 2021;24(1):7. https://doi.org/10.1208/s12248-021-00637-2 PMID: 34862519
38. Alfonso S, Jenner AL, Craig M. Translational approaches to treating dynamical diseases through in silico clinical trials. Chaos. 2020;30(12). https://doi.org/10.1063/5.0019556
39. Scott J. Phase i trialist. Lancet Oncol. 2012;13(3):236. https://doi.org/10.1016/s1470-2045(12)70098-0 PMID: 22489289
40. Polasek TM, Rostami-Hodjegan A. Virtual twins: understanding the data required for model-informed precision dosing. Clin Pharmacol Ther. 2020;107(4):742–5. https://doi.org/10.1002/cpt.1778 PMID: 32056199
41. Jenner AL, Cassidy T, Belaid K, Bourgeois-Daigneault M-C, Craig M. In silico trials predict that combination strategies for enhancing vesicular stomatitis oncolytic virus are determined by tumor aggressivity. J Immunother Cancer. 2021;9(2):e001387. https://doi.org/10.1136/jitc-2020-001387 PMID: 33608375
42. Wang H, Sové RJ, Jafarnejad M, Rahmeh S, Jaffee EM, Stearns V, et al. Conducting a virtual clinical trial in HER2-negative breast cancer using a quantitative systems pharmacology model with an epigenetic modulator and immune checkpoint inhibitors. Front Bioeng Biotechnol. 2020;8:141. https://doi.org/10.3389/fbioe.2020.00141 PMID: 32158754
43. Zahid MU, Mohamed ASR, Caudell JJ, Harrison LB, Fuller CD, Moros EG, et al. Dynamics-adapted radiotherapy dose (DARD) for head and neck cancer radiotherapy dose personalization. J Pers Med. 2021;11(11):1124. https://doi.org/10.3390/jpm11111124 PMID: 34834476
44. Kim E, Rebecca VW, Smalley KSM, Anderson ARA. Phase i trials in melanoma: a framework to translate preclinical findings to the clinic. Eur J Cancer. 2016;67:213–22. https://doi.org/10.1016/j.ejca.2016.07.024 PMID: 27689717
45. Allen RJ, Rieger TR, Musante CJ. Efficient generation and selection of virtual populations in quantitative systems pharmacology models. CPT Pharmacometrics Syst Pharmacol. 2016;5(3):140–6. https://doi.org/10.1002/psp4.12063 PMID: 27069777
46. Barish S, Ochs MF, Sontag ED, Gevertz JL. Evaluating optimal therapy robustness by virtual expansion of a sample population, with a case study in cancer immunotherapy. Proc Natl Acad Sci U S A. 2017;114(31):E6277–86. https://doi.org/10.1073/pnas.1703355114 PMID: 28716945
47. Jenner AL, Frascoli F, Yun C-O, Kim PS. Optimising Hydrogel release profiles for viro-immunotherapy using oncolytic adenovirus expressing IL-12 and GM-CSF with immature dendritic cells. Appl Sci. 2020;10(8):2872. https://doi.org/10.3390/app10082872
48. Jennera AL, Yun CO, Yoon A, Coster ACF, Kim PS. Modelling combined virotherapy and immunotherapy: strengthening the antitumour immune response mediated by IL-12 and GM-CSF expression. LiB. 2018;5(2). https://doi.org/10.30707/lib5.2jennera
49. Norton L. A Gompertzian model of human breast cancer growth. Cancer Res. 1988;48(24 Pt 1):7067–71. PMID: 3191483
50. Mahasa KJ, de Pillis L, Ouifki R, Eladdadi A, Maini P, Yoon A-R, et al. Mesenchymal stem cells used as carrier cells of oncolytic adenovirus results in enhanced oncolytic virotherapy. Sci Rep. 2020;10(1):425. https://doi.org/10.1038/s41598-019-57240-x PMID: 31949228
51. Ontah GM, Darti I, et al. Dynamic analysis of a tumor treatment model using oncolytic virus and chemotherapy with saturated infection rate. IOP Conference Series: Materials Science and Engineering; 2019. 32025 p. https://doi.org/10.1088/1757-899X/546/3/032025
52. Wodarz D, Komarova N. Towards predictive computational models of oncolytic virus therapy: basis for experimental validation and model selection. PLoS One. 2009;4(1):e4271. https://doi.org/10.1371/journal.pone.0004271 PMID: 19180240
53. Guo E, Dobrovolny HM. Mathematical modeling of oncolytic virus therapy reveals role of the immune response. Viruses. 2023;15(9):1812. https://doi.org/10.3390/v15091812 PMID: 37766219
54. Senekal NS, Mahasa KJ, Eladdadi A, de Pillis L, Ouifki R. Natural killer cells recruitment in oncolytic virotherapy: a mathematical model. Bull Math Biol. 2021;83(7):75. https://doi.org/10.1007/s11538-021-00903-6 PMID: 34008149
55. Malinzi J. A mathematical model for oncolytic virus spread using the telegraph equation. CNSNS. 2021;102:105944. https://doi.org/10.1016/j.cnsns.2021.105944
56. Wieland F-G, Hauber AL, Rosenblatt M, Tönsing C, Timmer J. On structural and practical identifiability. Curr Opin Syst Biol. 2021;25:60–9. https://doi.org/10.1016/j.coisb.2021.03.005
57. Raue A, Kreutz C, Maiwald T, Bachmann J, Schilling M, Klingmüller U, et al. Structural and practical identifiability analysis of partially observed dynamical models by exploiting the profile likelihood. Bioinformatics. 2009;25(15):1923–9. https://doi.org/10.1093/bioinformatics/btp358 PMID: 19505944

58. Eisenberg MC, Jain HV. A confidence building exercise in data and identifiability: modeling cancer chemotherapy as a case study. J Theor Biol. 2017;431:63–78. https://doi.org/10.1016/j.jtbi.2017.07.018 PMID: 28733187
59. Brady R, Enderling H. Mathematical models of cancer: when to predict novel therapies, and when not to. Bull Math Biol. 2019;81(10):3722–31. https://doi.org/10.1007/s11538-019-00640-x PMID: 31338741
60. Chis O-T, Banga JR, Balsa-Canto E. Structural identifiability of systems biology models: a critical comparison of methods. PLoS One. 2011;6(11):e27755. https://doi.org/10.1371/journal.pone.0027755 PMID: 22132135
61. Simpson MJ, Browning AP, Warne DJ, Maclaren OJ, Baker RE. Parameter identifiability and model selection for sigmoid population growth models. J Theor Biol. 2022;535:110998. https://doi.org/10.1016/j.jtbi.2021.110998 PMID: 34973274
62. Bellu G, Saccomani MP, Audoly S, D'Angiò L. DAISY: a new software tool to test global identifiability of biological and physiological systems. Comput Methods Programs Biomed. 2007;88(1):52–61. https://doi.org/10.1016/j.cmpb.2007.07.002 PMID: 17707944
63. Saccomani MP, Bellu G, Audoly S, d'Angió L. A new version of DAISY to test structural identifiability of biological models. Computational Methods in Systems Biology: 17th International Conference, CMSB 2019; 2019 Sept 18–20; Trieste, Italy, Proceedings 17; 2019. p. 329–34. https://doi.org/10.1007/978-3-030-31304-3_21
64. Hines KE, Middendorf TR, Aldrich RW. Determination of parameter identifiability in nonlinear biophysical models: a Bayesian approach. J Gen Physiol. 2014;143(3):401–16. https://doi.org/10.1085/jgp.201311116 PMID: 24516188
65. Toni T, Welch D, Strelkowa N, Ipsen A, Stumpf MPH. Approximate Bayesian computation scheme for parameter inference and model selection in dynamical systems. J R Soc Interface. 2009;6(31):187–202. https://doi.org/10.1098/rsif.2008.0172 PMID: 19205079
66. Minter A, Retkute R. Approximate Bayesian Computation for infectious disease modelling. Epidemics. 2019;29:100368. https://doi.org/10.1016/j.epidem.2019.100368 PMID: 31563466
67. Malvehy J, Samoylenko I, Schadendorf D, Gutzmer R, Grob J-J, Sacco JJ, et al. Talimogene laherparepvec upregulates immune-cell populations in non-injected lesions: findings from a phase II, multicenter, open-label study in patients with stage IIIB-IVM1c melanoma. J Immunother Cancer. 2021;9(3):e001621. https://doi.org/10.1136/jitc-2020-001621 PMID: 33785610
68. Heidbuechel JPW, Engeland CE. Paramyxoviruses for tumor-targeted immunomodulation: design and evaluation ex vivo. J Vis Exp. 2019;(143):e58651. https://doi.org/10.3791/58651 PMID: 30663684
69. Leick KM, Pinczewski J, Mauldin IS, Young SJ, Deacon DH, Woods AN, et al. Patterns of immune-cell infiltration in murine models of melanoma: roles of antigen and tissue site in creating inflamed tumors. Cancer Immunol Immunother. 2019;68(7):1121–32. https://doi.org/10.1007/s00262-019-02345-5 PMID: 31134297
70. Andtbacka RHI, Kaufman HL, Collichio F, Amatruda T, Senzer N, Chesney J, et al. Talimogene laherparepvec improves durable response rate in patients with advanced melanoma. J Clin Oncol. 2015;33(25):2780–8. https://doi.org/10.1200/JCO.2014.58.3377 PMID: 26014293
71. Del Monte U. Does the cell number 10(9) still really fit one gram of tumor tissue? Cell Cycle. 2009;8(3):505–6. https://doi.org/10.4161/cc.8.3.7608 PMID: 19176997
72. Elmore S. Apoptosis: a review of programmed cell death. Toxicol Pathol. 2007;35(4):495–516. https://doi.org/10.1080/01926230701320337 PMID: 17562483
73. Dela A, Shtylla B, de Pillis L. Multi-method global sensitivity analysis of mathematical models. J Theor Biol. 2022;546:111159. https://doi.org/10.1016/j.jtbi.2022.111159 PMID: 35577102
74. Yankeelov TE, Hormuth DA 2nd, Lima EABF, Lorenzo G, Wu C, Okereke LC, et al. Designing clinical trials for patients who are not average. iScience. 2023;27(1):108589. https://doi.org/10.1016/j.isci.2023.108589 PMID: 38169893
75. Dessinioti C, Plaka M, Befon A, Polidorou D, Stefanaki I, Kypreou K, et al. A retrospective study of diameter and Breslow thickness in invasive melanomas. Dermatology. 2024;240(3):462–7. https://doi.org/10.1159/000536151 PMID: 38290473
76. Rohatgi A. WebPlotDigitizer. Available from: https://automeris.io
77. Simon G, et al. 762 First-in-human phase 1a study of NG-641, a tumour-selective vector expressing a FAP-TAc bispecific antibody and immune enhancer module, in patients with metastatic/advanced epithelial tumours (STAR). BMJ Specialist J. 2022.
78. Lillie T, et al. NEBULA: A multicenter phase 1a/b study of a tumor-selective transgene-expressing adenoviral vector, NG-641, and nivolumab in patients with metastatic or advanced epithelial tumors. 2022.
79. Packiriswamy N, Upreti D, Zhou Y, Khan R, Miller A, Diaz RM, et al. Oncolytic measles virus therapy enhances tumor antigen-specific T-cell responses in patients with multiple myeloma. Leukemia. 2020;34(12):3310–22. https://doi.org/10.1038/s41375-020-0828-7 PMID: 32327728
80. Labrijn AF, Janmaat ML, Reichert JM, Parren PWHI. Bispecific antibodies: a mechanistic review of the pipeline. Nat Rev Drug Discov. 2019;18(8):585–608. https://doi.org/10.1038/s41573-019-0028-1 PMID: 31175342
81. Klein C, Brinkmann U, Reichert JM, Kontermann RE. The present and future of bispecific antibodies for cancer therapy. Nat Rev Drug Discov. 2024;23(4):301–19. https://doi.org/10.1038/s41573-024-00896-6 PMID: 38448606
82. Choi BD, Yu X, Castano AP, Bouffard AA, Schmidts A, Larson RC, et al. CAR-T cells secreting BiTEs circumvent antigen escape without detectable toxicity. Nat Biotechnol. 2019;37(9):1049–58. https://doi.org/10.1038/s41587-019-0192-1 PMID: 31332324
83. Velasquez MP, Torres D, Iwahori K, Kakarla S, Arber C, Rodriguez-Cruz T, et al. T cells expressing CD19-specific engager molecules for the immunotherapy of CD19-positive malignancies. Sci Rep. 2016;6:27130. https://doi.org/10.1038/srep27130 PMID: 27255991

84. Hao S, Inamdar VV, Sigmund EC, Zhang F, Stephan SB, Watson C, et al. BiTE secretion from in situ-programmed myeloid cells results in tumor-retained pharmacology. J Control Release. 2022;342:14–25. https://doi.org/10.1016/j.jconrel.2021.12.029 PMID: 34953983

85. Engeland CE, Grossardt C, Veinalde R, Bossow S, Lutz D, Kaufmann JK, et al. CTLA-4 and PD-L1 checkpoint blockade enhances oncolytic measles virus therapy. Mol Ther. 2014;22(11):1949–59. https://doi.org/10.1038/mt.2014.160 PMID: 25156126

86. Philipp N, Kazerani M, Nicholls A, Vick B, Wulf J, Straub T, et al. T-cell exhaustion induced by continuous bispecific molecule exposure is ameliorated by treatment-free intervals. Blood. 2022;140(10):1104–18. https://doi.org/10.1182/blood.2022015956 PMID: 35878001

87. Wang J, Huang X, Shi Q, Swingle KL, Hamilton AG, Gong N, et al. Drug-loaded bispecific T cell nanoengager overcomes T cell exhaustion for potent cancer immunotherapy. Proc Natl Acad Sci U S A. 2025;122(45):e2409564122. https://doi.org/10.1073/pnas.2409564122 PMID: 41183182

88. van de Donk NWCJ, Chari A, Mateos MV. Mechanisms of resistance against T-cell engaging bispecific antibodies in multiple myeloma: implications for novel treatment strategies. Lancet Haematol. 2024;11(9):e693–707. https://doi.org/10.1016/S2352-3026(24)00186-8 PMID: 39033769

89. Dobrovolny HM. Mathematical modeling of virus-mediated syncytia formation: past successes and future directions. In: Syncytia: origin, structure, and functions; 2023. p. 345–70. https://doi.org/10.1007/978-3-031-37936-9_17

90. Berg DR, Offord CP, Kemler I, Ennis MK, Chang L, Paulik G, et al. In vitro and in silico multidimensional modeling of oncolytic tumor virotherapy dynamics. PLoS Comput Biol. 2019;15(3):e1006773. https://doi.org/10.1371/journal.pcbi.1006773 PMID: 30835721